iScience

CellPress
OPEN ACCESS

Article

Dissecting the concordant and disparate roles of NDUFAF3 and NDUFAF4 in mitochondrial complex I biogenesis

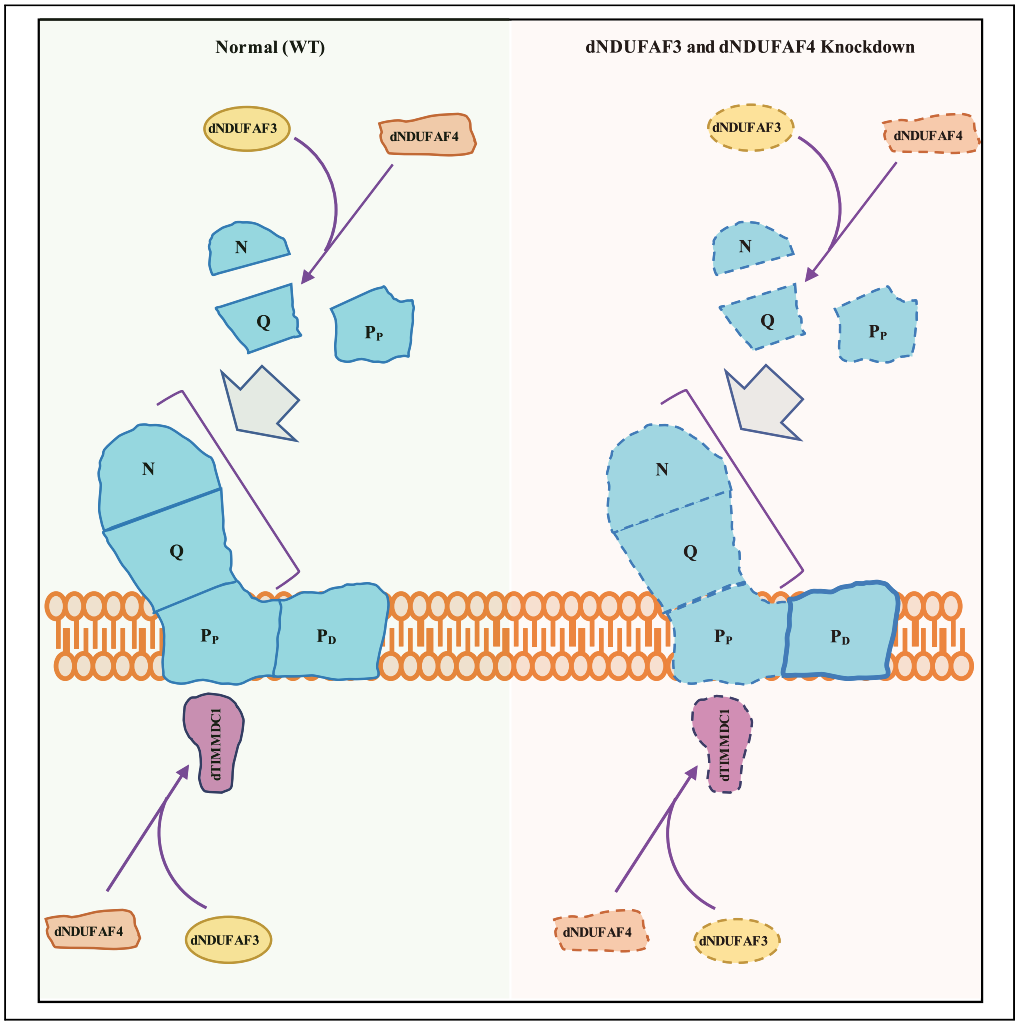

Anjaneyulu Murari, Shauna-Kay Rhooms, Christian Garcia, ..., Bibhuti Mishra, Cassie Deshong, Edward Owusu-Ansah

eo2364@cumc.columbia.edu

Highlights

Disruption of NDUFAF3 and NDUFAF4 in Drosophila muscles destabilizes TIMMDC1

NDUFAF3 and NDUFAF4 regulate biogenesis of the N, Q, and Pp modules

NDUFAF4 ameliorates some of the CI biogenesis defects in NDUFAF3 mutants

Murari et al., iScience 24, 102869
August 20, 2021
https://doi.org/10.1016/j.isci.2021.102869

iScience

CellPress
OPEN ACCESS

Article

Dissecting the concordant and disparate roles of NDUFAF3 and NDUFAF4 in mitochondrial complex I biogenesis

Anjaneyulu Murari,[1] Shauna-Kay Rhooms,[1] Christian Garcia,[1] Tong Liu,[2] Hong Li,[2] Bibhuti Mishra,[1] Cassie Deshong,[1] and Edward Owusu-Ansah[1,3,4,*]

SUMMARY

Distinct sub-assemblies (modules) of mitochondrial complex I (CI) are assembled with the assistance of CI Assembly Factors (CIAFs) through mechanisms that are incompletely defined. Here, using genetic analyses in *Drosophila*, we report that when either of the CIAFs – NDUFAF3 or NDUFAF4 – is disrupted, biogenesis of the Q-, N-, and P_{P-b}-modules of CI is impaired. This is due, at least in part, to the compromised integration of NDUFS3 and NDUFS5 into the Q-, and P_{P-b}-modules, respectively, coupled with a destabilization of another CIAF, TIMMDC1, in assembly intermediates. Notably, forced expression of NDUFAF4 rescues the biogenesis defects in the Q-module and some aspects of the defects in the P_{P-b}-module of CI when NDUFAF3 is disrupted. Altogether, our studies furnish new fundamental insights into the mechanism by which NDUFAF3 and NDUFAF4 regulate CI assembly and raises the possibility that certain point mutations in NDUFAF3 may be rescued by overexpression of NDUFAF4.

INTRODUCTION

NADH:ubiquinone oxidoreductase, more commonly referred to as mitochondrial complex I (CI), is the largest holoenzyme of the oxidative phosphorylation system (OXPHOS). Mammalian CI has 44 distinct subunits and is tightly intertwined with a dozen or so phospholipid molecules. It also has 8 Fe-S clusters, two phosphopantetheine molecules, and a molecule each of NADPH, Zn^{2+}, and flavin mononucleotide (FMN) (Fiedorczuk et al., 2016; Letts et al. 2016; Letts and Sazanov 2017; Agip et al., 2018). These seemingly disparate components must be incorporated together in a precise orientation to form a functioning enzyme. In addition, one of the subunits (NDUFAB1) occurs twice in the complex, resulting in a total of 45 subunits of CI. The two copies of NDUFAB1 must be inserted into two distinct portions of the complex during the assembly process. Consequently, CI assembly is a highly regulated process, with many of the mechanistic molecular details still unclear.

Fourteen of the 45 subunits form the catalytic centers of the enzyme. Accordingly, they are referred to as the core or central subunits of CI (Fiedorczuk et al., 2016; Baradaran et al., 2013; Vinothkumar et al. 2014; J. Zhu, Vinothkumar, and Hirst 2016). 7 core subunits are encoded in the nucleus (i.e. NDUFS1, NDUFS2, NDUFS3, NDUFS7, NDUFS8, NDUFV1, and NDUFV2), while the other 7 are encoded by mtDNA (i.e. ND1, ND2, ND3, ND4, ND4L, ND5, and ND6). The 31 (30 distinct) remaining subunits are also encoded by nuclear DNA and are referred to as accessory or supernumerary subunits. There are two major domains of CI that regulate its two bioenergetic functions. The two domains are a hydrophobic proton-pumping membrane-localized domain, and a hydrophilic electron-transferring peripheral domain that juts into the mitochondrial matrix. These two domains of CI are oriented almost perpendicularly to each other, giving rise to the boot-shaped structure of CI (Baradaran et al., 2013; Efremov and Sazanov 2011).

During CI biogenesis, transient assembly intermediates (AIs) consisting of a few CI subunits are formed largely independently of other CI AIs. The CI AIs or subcomplexes ultimately merge with each other or other subunits to form the mature complex. Additionally, about a dozen or so CIAFs have been identified. CIAFs are proteins that are usually found in association with specific subcomplexes and assist with the assembly process, but are subsequently released when assembly is complete. Some CIAFs function as chaperones to stabilize specific CI subcomplexes or assist with the combination of two subcomplexes to form a

[1]Department of Physiology and Cellular Biophysics, Columbia University Irving Medical Center, New York, NY 10032, USA

[2]Center for Advanced Proteomics Research, Department of Microbiology, Biochemistry and Molecular Genetics, Rutgers University - New Jersey Medical School, Newark, NJ 07103, USA

[3]The Robert N. Butler Columbia Aging Center, Columbia University Irving Medical Center, New York, NY 10032, USA

[4]Lead contact

*Correspondence: eo2364@cumc.columbia.edu

https://doi.org/10.1016/j.isci.2021.102869

larger subcomplex. Others have more specific roles: such as regulating a post-translational modification on a specific CI subunit, as is the case for NDUFAF5 and NDUFAF7 (reviewed in (Formosa et al., 2018)). There are also regulators of CI assembly that have more global effects on OXPHOS assembly. Such is the case for apoptosis-inducing factor, which regulates the intramitochondrial transport of some components of the mitochondrial contact site and cristae organizing system, thereby influencing CI assembly indirectly (Murari et al., 2020). A thorough characterization of the roles of all CIAFs is required as it will improve our understanding of CI assembly, and possibly, uncover new therapeutic options for mitochondrial CI diseases.

Some CI AIs consist of sub-assemblies that form the 3 functional modules of CI (the N, Q, and P-modules). Located at the most distal part of the matrix domain, the N-module is the site of NADH oxidation and contains the FMN prosthetic group. The Q-module connects the N module to the membrane domain and transfers electrons through Fe-S clusters to ubiquinone (reviewed in (Rhooms et al., 2019)). The N- and Q-modules together form the matrix domain. The membrane domain is essentially comprised of the proton-pumping P-module. The P-module can be further subdivided into a proximal P_P module and a distal P_D module; as the P_P and P_D modules are proximal and distal to the region of attachment of the matrix and membrane domains, respectively. Studies in mammalian cells have shown that during CI biogenesis, the P_P module is assembled from two sub-modules (i.e. the $P_{P\text{-}a}$ and $P_{P\text{-}b}$ sub-modules). Similarly, the P_D module is preassembled as separate $P_{D\text{-}a}$ and $P_{D\text{-}b}$ sub-modules, which eventually merge with each other to form the P_D module. Thus, commencing at the region where the membrane and matrix domains adjoin, and progressing distally, the P-module consists of the $P_{P\text{-}a}$, $P_{P\text{-}b}$, $P_{D\text{-}a}$, and $P_{D\text{-}b}$ sub-modules (reviewed in (Sánchez-Caballero et al. 2016)). The $P_{P\text{-}a}$, $P_{P\text{-}b}$, $P_{D\text{-}a}$, and $P_{D\text{-}b}$ sub-modules are essentially analogous to the ND1, ND2, ND4, and ND5 sub-modules, respectively (reviewed in (Formosa et al., 2018)).

Mutations in both NADH dehydrogenase 1 alpha subcomplex assembly factor 3 (NDUFAF3, also referred to as C3ORF60) and NADH dehydrogenase 1 alpha subcomplex assembly factor 4 (NDUFAF4, also referred to as C6ORF66) have long been associated with Leigh Syndrome (Baertling et al., 2017a, 2017b). NDUFAF4 was discovered by homozygosity mapping of patients who presented with symptoms of CI deficiency, while NDUFAF3 was discovered by phylogenetic profiling to uncover proteins that co-evolved with CI and are consequently lost in organisms without CI (Saada et al., 2008; Pagliarini et al., 2008). Further studies identified patients with mutations in NDUFAF3 (Saada et al., 2009). Immunoblotting and proteomic analyses have revealed the co-migration of NDUFAF3 and NDUFAF4 with at least 5 CI subunits: NDUFS2, NDUFS3, NDUFS7, NDUFS8, and NDUFA5. As these 5 CI subunits are part of the Q-module, this observation is consistent with a role of NDUFAF3 and NDUFAF4 in regulating the assembly or ensuring the stability of the Q-module during the CI assembly process (Saada et al., 2009; Guerrero-Castillo et al., 2017). However, whether NDUFAF3 or NDUFAF4 can regulate the biogenesis of other CI modules or whether mutations in NDUFAF3 or NDUFAF4 can be rescued by the upregulation of NDUFAF4 or NDUFAF3, respectively, was hitherto unknown.

We previously reported that the mechanism of CI assembly in *Drosophila* flight (thoracic) muscles correlates with what has been described in mammalian systems (Garcia et al., 2017; Rhooms et al., 2019). This, coupled with its classical genetics, make *Drosophila* an ideal model system for dissecting the mechanism by which various CIAFs regulate CI assembly *in vivo*. Accordingly, we sought to define the effect of disrupting NDUFAF3 and NDUFAF4 on the expression of other CIAFs, and the biogenesis of specific modules of CI. We find that RNAi-mediated knockdown of the *Drosophila* ortholog of NDUFAF3 or NDUFAF4 inhibits the biogenesis of the Q-, N-, and $P_{P\text{-}b}$-modules of CI. This is associated with a reduction in the amount of NDUFS3, NDUFV3, and NDUFS5 that incorporates into the Q-, N-, and $P_{P\text{-}b}$-modules, respectively. In addition, knockdown of NDUFAF3 or NDUFAF4 reduces the amount of TIMMDC1 associated with AIs. Remarkably, forced expression of NDUFAF4, rescues the diminished integration of NDUFS3 and NDUFS5 into the Q- and $P_{P\text{-}b}$ modules of CI when NDUFAF3 is disrupted. Our work raises the possibility that certain mutations in NDUFAF3 may be rescued by overexpression of NDUFAF4.

RESULTS

RNAi-mediated disruption of *Drosophila* orthologs of NDUFAF3 and NDUFAF4 in flight muscles impairs complex I assembly but increases complex II and complex IV activity

A search on the Ensembl genome browser revealed that *Drosophila* orthologs of NDUFAF3 and NDUFAF4 are CG5569 and CG11722, respectively. For simplicity, we refer to CG5569 and CG11722 as dNDUFAF3 and dNDUFAF4, respectively, and prefix all *Drosophila* orthologs of CI subunits and CIAFs with "d"

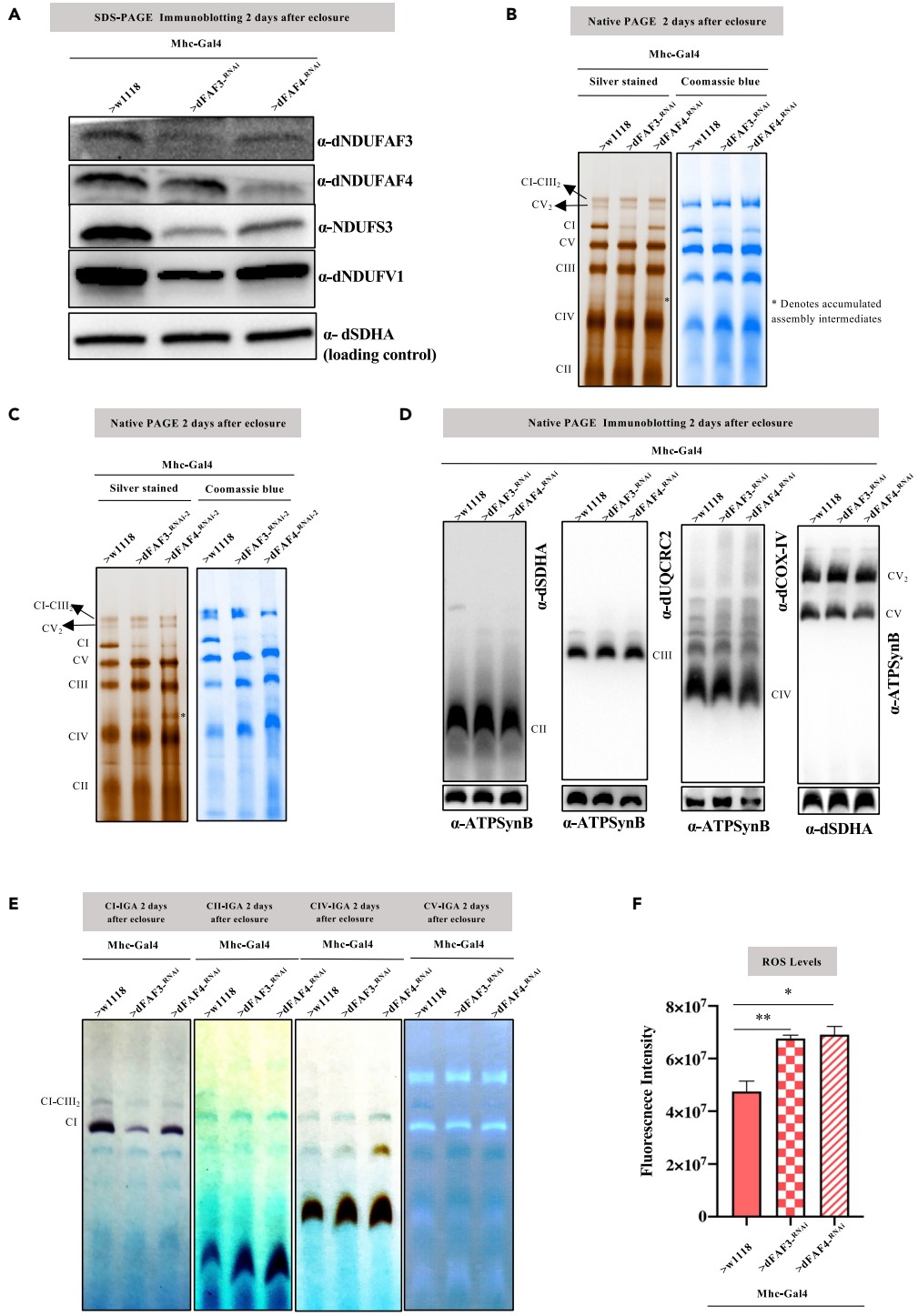

Figure 1. RNAi-mediated disruption of *Drosophila* orthologs of NDUFAF3 and NDUFAF4 in flight muscles impairs complex I assembly but increases complex II and complex IV activity

(A) Total cell lysates from flight/thoracic muscles isolated from adult flies expressing the transgenic RNAi constructs shown in muscles (using Mhc-Gal4) 2 days post-eclosure, were analyzed by SDS-PAGE and anti-dNDUFAF3, anti-dNDUFAF4, anti-NDUFS3, anti-dNDUFV1, and anti-dSDHA immunoblotting. Anti-dSDHA was used as a loading control.

(B) Mitochondrial preparations from adult thoracic muscles expressing the transgenic RNAi constructs shown 2 days after eclosure, were analyzed by silver staining of native gels and blue native polyacrylamide gel electrophoresis (BN-PAGE). The asterisk (*) denotes accumulated assembly intermediates.

Figure 1. *Continued*
(C) Similar to (B) but with an independent set of transgenic RNAi constructs to dNDUFAF3 and dNDFUFAF4.
(D) Immunoblotting of native OXPHOS complexes in mitochondrial preparations from flight muscles expressing the transgenic RNAi constructs shown in muscles.
(E) Complex I, complex II, complex IV, and complex V in-gel activity assays of OXPHOS complexes obtained from mitochondrial preparations from flight muscles of flies with the genotypes shown.
(F) ROS levels in mitochondrial preparations from thoraces of Mhc-Gal4/w1118 (wild-type), Mhc-Gal4/UAS-dNDUFAF3^{-RNAi}, and Mhc-Gal4/UAS-dNDUFAF4^{-RNAi} flies relative to wild-type controls 2 days post-eclosure. n = 3 biological replicates with 40 flies per replicate; p values are based on the student's t-test for unpaired two-tailed samples. The fold change shown refers to the mean ± s.e.m (standard error of the mean); and n.s. denotes $p > 0.05$, * = $p < 0.05$, ** = $p < 0.01$ and *** = $p < 0.001$.
See also Figure S1.

(as in dNDUFAF3 for NDUFAF3, etc) elsewhere in this manuscript. We knocked down the expression of dNDUFAF3 and dNDUFAF4 in thoracic muscles using the Gal4/UAS system (Brand and Perrimon 1993). No adult flies were recovered with the more potent Dmef2-Gal4 driver that is expressed in muscles throughout development. However, viable flies were obtained when the expression of dNDUFAF3 or dNDUFAF4 in thoracic muscles were knocked down with the Mhc-Gal4 driver. Immunoblotting analyses indicated that dNDUFAF3 and dNDUFAF4 expression had been significantly attenuated in thoraces dissected from the *Mhc-Gal4/UAS-dNDUFAF3^{-RNAi}* (FAF3-kd) and *Mhc-Gal4/UAS-dNDUFAF4^{-RNAi}* (FAF4-kd) flies respectively, relative to wildtype controls (i.e. *Mhc-Gal4/w1118*) (Figure 1A).

To evaluate the effect of disrupting dNDUFAF3 and dNDUFAF4 on the assembly of OXPHOS complexes in adult flight muscles, we isolated mitochondria from thoraxes of FAF3-kd and FAF4-kd flies, solubilized their membranes in digitonin, and evaluated the integrity of their OXPHOS complexes using silver staining and blue native polyacrylamide gel electrophoresis (BN-PAGE). The assembly of CI was impaired in mitochondria from thoraces, where dNDUFAF3 or dNDUFAF4 expression was knocked down using MhcGal4 (Figures 1B and S1). Similar results were obtained when different transgenic RNAi constructs targeting *dNDUFAF3* and *dNDUFAF4* were used (Figure 1C). Immunoblotting of OXPHOS complexes, using the antibodies indicated, revealed that CII through CV were assembled normally in thoraxes of FAF3-kd and FAF4-kd flies (Figure 1D). In-gel CI activity was reduced when the expression of dNDUFAF3 or dNDUFAF4 was knocked down, in agreement with observations from Figures 1B and 1C (Figure 1E). Although immunoblotting of the OXPHOS complexes revealed that the extent of expression of dSDHA and dCOX-IV was not appreciably different between the wild-type samples and samples where dNDUFAF3 and dNDUFAF4 were knocked down (Figure 1D); in-gel CII and CIV activity were actually higher in thoraxes of FAF3-kd and FAF4-kd flies, relative to wild-type, while in-gel CV activity was not appreciably affected (Figure 1E). In addition, an Amplex Red assay revealed that the amount of reactive oxygen species (ROS) produced in FAF3-kd and FAF4-kd thoraxes was elevated relative to wild-type controls (Figure 1F).

In view of the fact that CII and CIV were assembled to the same extent in wild-type and FAF3-kd and FAF4-kd flies, it is possible that the increased CII and CIV in-gel activities are due to post-translational modifications on some CII and CIV subunits that enhance their activities. Altogether, these results indicate that the *Drosophila* orthologs of NDUFAF3 and NDUFAF4 regulate the assembly of CI in adult thoracic muscles and induce a compensatory adaptive response involving increased CII and CIV activity when genetically disrupted. Thus, the flight muscles of *Drosophila* are a suitable system to explore the AI profile of FAF3-kd and FAF4-kd flies, and whether genetic disruption of *dNDUFAF3* or *dNDUFAF4* can be rescued by the upregulation of dNDUFAF4 or dNDUFAF3, respectively.

The synthesis of some CI AIs localized to the mitochondrial matrix are stalled when dNDUFAF4 or dNDUFAF3 is disrupted

As a first step toward unraveling the mechanism by which dNDUFAF3 and dNDUFAF4 regulate CI assembly, we analyzed the effect of disrupting these two CIAFs on biogenesis of the matrix-localized modules of CI. The two functional modules of CI situated in the part of CI that extends into the mitochondrial matrix are the Q- and N-modules (Figures S2 and 2A). Biogenesis of the Q-module begins with the formation of an AI consisting of dNDUFS2 and dNDUFS3, which subsequently combines with dNDUFS7 and dNDUFS8. Therefore, we used an antibody that detects dNDUFS3 (anti-NDUFS3) to track the incorporation of dNDUFS3 into the Q module by immunoblotting of blue native gels.

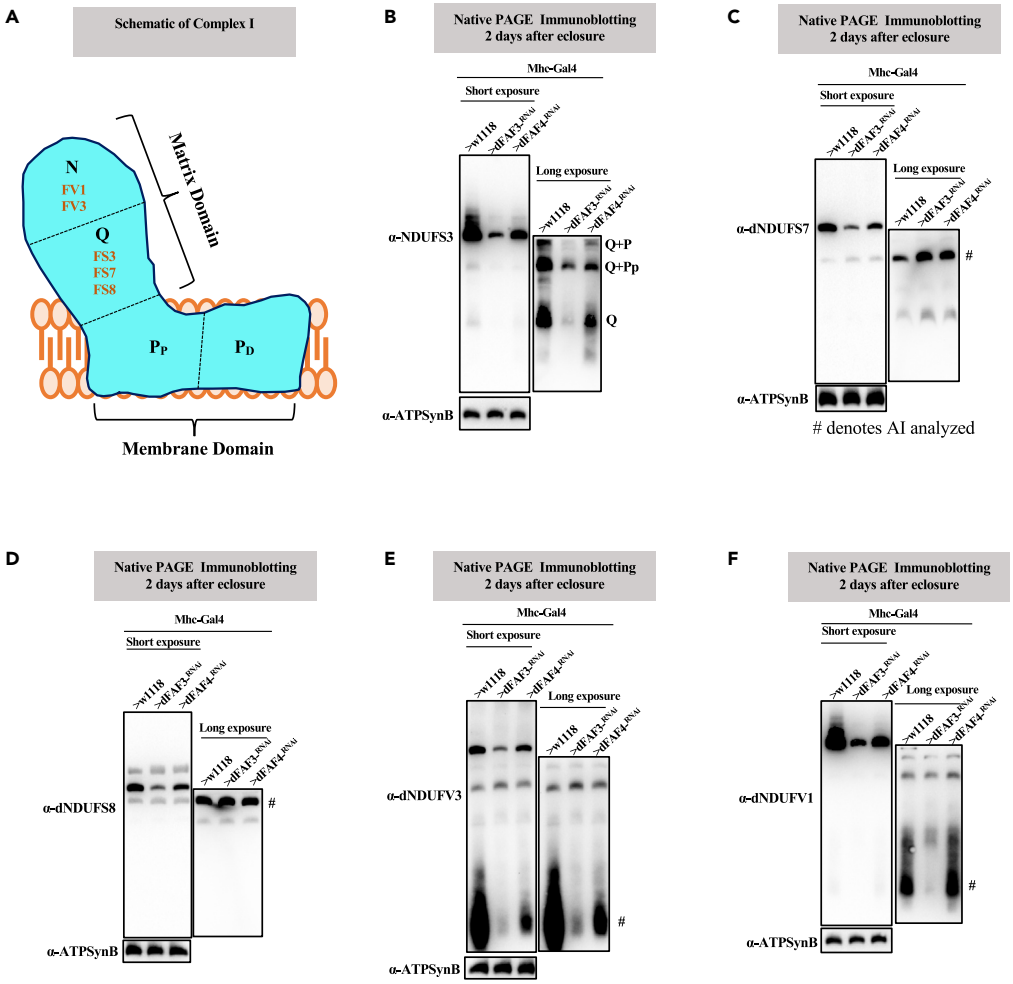

Figure 2. The synthesis of some CI assembly intermediates localized to the mitochondrial matrix are stalled when dNDUFAF4 or dNDUFAF3 is disrupted

(A) A diagram depicting the boot-shaped structure of mitochondrial CI in the mitochondrial inner membrane and the approximate positions of the N, Q, P_P, and P_D modules. The matrix and membrane domains are oriented almost perpendicularly to each other. A commercially available antibody that detects dNDUFS3 (FS3), and antibodies we raised against dNDUFS7 (FS7) and dNDUFS8 (FS8) were used to track the biogenesis of the Q-module. Biogenesis of the N-module was monitored by immunoblotting with antibodies we raised against dNDUFV1 (FV1) and dNDUFV3 (FV3).

(B–F) Mitochondrial preparations from thoraces isolated from Mhc-Gal4/w1118 (wild-type), Mhc-Gal4/UAS-dNDUFAF3^{-RNAi}, and Mhc-Gal4/UAS-dNDUFAF4^{-RNAi} flies 2 days after eclosure were analyzed by BN-PAGE, followed by immunoblotting with the antibodies indicated. The blots were imaged following a short exposure to detect the holoenzyme and supercomplexes, after which the region corresponding to the holoenzyme and supercomplexes was cut off, and the rest of the blot re-imaged after a longer exposure to detect the assembly intermediates. The antibodies used were anti-NDUFS3 which detects dNDUFS3 (B), anti-dNDUFS7 (C), anti-dNDUFS8 (D), anti-dNDUFV3 (E), and anti-dNDUFV1 (F). Anti-ATP Synthase Beta (ATP5F1B) which detects the *Drosophila* ortholog, dATP-Synβ was used as a loading control.

See also Figure S2.

We observed that the extent of incorporation of dNDUFS3 into the Q module was diminished in both FAF3-kd and FAF4-kd flies (Figure 2B). Additionally, there was a notable accumulation of a dNDUFS7-containing subcomplex in mitochondria from FAF3-kd and FAF4-kd thoraces, perhaps reflecting the continued incorporation of dNDUFS7 into the stalled and dysfunctional Q-module (Figure 2C). On the contrary, a subcomplex containing dNDUFS8, which is another core/central subunit of CI, and is part of the Q module, was not appreciably affected in either FAF3-kd or FAF4-kd flies (Figure 2D).

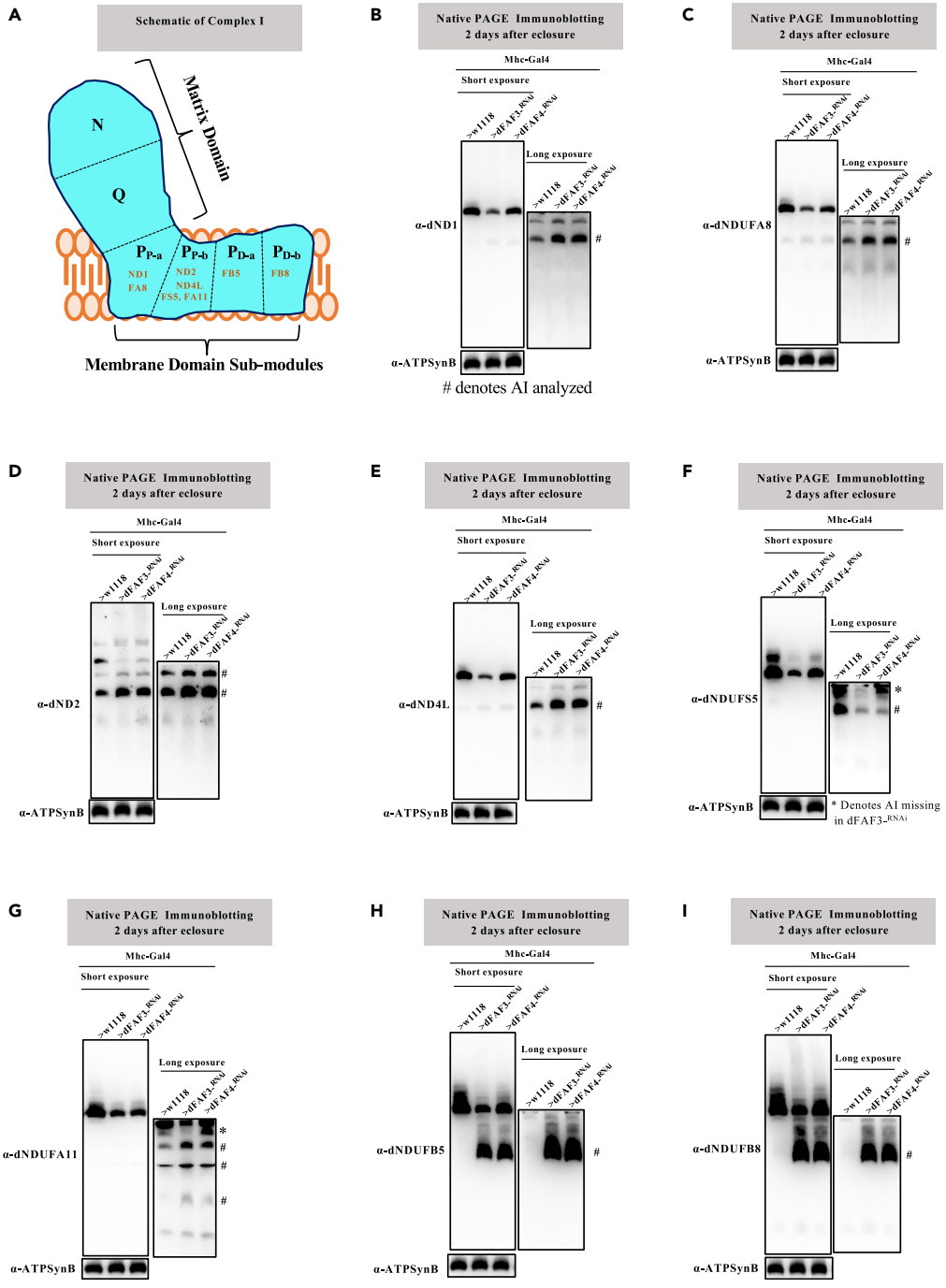

Figure 3. The biogenesis of some assembly intermediates in the mitochondrial inner membrane are stalled when dNDUFAF4 or dNDUFAF3 is disrupted

(A) A representation of mitochondrial CI showing the approximate positions of the N and Q modules, as well as the sub-modules in the membrane domain. The P_P and P_D modules can be further subdivided into the $P_{P\text{-}a}$, $P_{P\text{-}b}$, $P_{D\text{-}a}$ and $P_{D\text{-}b}$ sub-modules. Antibodies raised against the subunits shown were used to track the synthesis of the various sub-modules.

(B–I) Mitochondrial preparations from thoraces isolated from flies with the genotypes indicated 2 days after eclosure were analyzed by BN-PAGE, followed by immunoblotting with the antibodies listed. The blots were imaged following a short exposure to detect the holoenzyme and supercomplexes, after which the region corresponding to the holoenzyme and supercomplexes was cut off, and the rest of the blot re-imaged after a longer exposure to detect the assembly

Figure 3. *Continued*
intermediates. The antibodies used were anti-dND1 (B), anti-dNDUFA8 (C), anti-dND2 (D), anti-dND4L (E), dNDUFS5 (F), anti-dNDUFA11 (G), anti-dNDUFB5 (H), and anti-dNDUFB8 (I). Anti-ATP Synthase Beta (ATP5F1B) which detects the *Drosophila* ortholog, dATP-Synβ was used as a loading control.
See also Figure S2.

As dNDUFV1 and dNDUFV3 are part of the N-module (Figure 2A), we tracked the incorporation of these two subunits into CI subcomplexes to monitor the integrity of the N module. The level of incorporation of dNDUFV3 into a subcomplex containing dNDUFV3 was strongly reduced in thoraxes from FAF3-kd and FAF4-kd flies (Figure 2E). A pronounced difference was observed between FAF3-kd and FAF4-kd flies with respect to the extent of assimilation of dNDUFV1 into a subcomplex of the N module, as incorporation of dNDUFV1 was reduced in FAF3-kd thoraces but was relatively unaffected in FAF4-kd thoraces at this stage (Figure 2F). Thus, although proteomic analyses has revealed the co-migration of dNDUFAF3 and dNDUFAF4 with essentially all the Q-module subunits (Guerrero-Castillo et al., 2017), the primary function of both dNDUFAF3 and dNDUFAF4 with regard to regulating the synthesis of the Q-module is to regulate incorporation of dNDUFS3 into the Q-module.

The biogenesis of some AIs in the mitochondrial inner membrane are stalled when dNDUFAF4 or dNDUFAF3 is disrupted

We explored whether dNDUFAF3 and dNDUFAF4 regulate the biogenesis of some of the membrane-localized subcomplexes of CI. The membrane domain – comprising of the P-module – can be sub-divided into a proximal (P_P) and a distal (P_D) domain; each of which can be further split into a pair of sub-modules (Figures S2 and 3A). The 7 mtDNA-encoded CI subunits (i.e. ND1, ND2, ND3, ND4, ND4L, ND5, and ND6) are part of the P-module. Nuclear-encoded CI subunits that are assembled together with ND1, ND2, ND4, and ND5 into the membrane define the 4 sub-modules of the P-module. Accordingly, the P_P module can be further split into the $P_{P\text{-}a}$ and $P_{P\text{-}b}$ sub-modules that contain ND1 and ND2, respectively; while the P_D module consists of the $P_{D\text{-}a}$ and $P_{D\text{-}b}$ sub-modules within which ND4 and ND5 are assembled, respectively (Figures S2 and 3A) (reviewed in (Sánchez-Caballero et al. 2016; Formosa et al., 2018)). Immunoblotting of CI subcomplexes using antibodies raised against subunits in the $P_{P\text{-}a}$ sub-module, such as dND1 and dNDUFA8, revealed that there was an accretion of a subcomplex containing these two subunits in FAF3-kd and FAF4-kd flies (Figures 3B and 3C). Similarly, with regard to subunits in the $P_{P\text{-}b}$ sub-module, there was a build-up of dND2-and dND4L-containing subcomplexes (Figures 3D and 3E). In contrast to these observations, the amount of dNDUFS5 that had incorporated into the $P_{P\text{-}b}$ sub-module was reduced in both FAF3-kd and FAF4-kd samples, relative to wild-type controls (Figure 3F).

We note that the $P_{P\text{-}b}$ sub-module subcomplex phenotype of FAF3-kd and FAF4-kd were not exactly the same. In FAF3-kd samples, at least two FS5-containing subcomplexes were impaired in FAF3-kd samples, while only the smaller of the two FS5-containing subcomplexes was impaired in FAF4-kd samples (Figure 3F). The larger subcomplex that is attenuated in FAF3-kd samples but present in FAF4-kd samples was reproduced by immunoblotting with an antibody that detects dNDUFA11, another nuclear-encoded subunit in the $P_{P\text{-}b}$ sub-module (Figure 3G). We refer to this large subcomplex that migrates just below the CI holoenzyme as the terminal AI (AI-T). Furthermore, although anti-dNDUFB5 and anti-dNDUFB8 immunoblotting of samples revealed that the $P_{D\text{-}a}$ and $P_{D\text{-}b}$ sub-modules do not accumulate in wild-type samples, there was a robust accumulation of dNDUFB5- and dNDUFB8-containing subcomplexes in samples from FAF3-kd and FAF4-kd flies (Figures 3H and 3I). Taken as a whole, these results show that the dysfunctional Q-module formed is associated with a bottleneck in the biogenesis of the P-module as well. Thus, in addition to their roles in regulating the biogenesis of the Q-module, dNDUFAF3 and dNDUFAF4 regulate the incorporation of dNDUFS5 into the $P_{P\text{-}b}$ sub-module; or the stabilization of dNDUFS5 once incorporated into the $P_{P\text{-}b}$ sub-module is dependent on dNDUFAF3 and dNDUFAF4.

Proteomic analyses to identify the constituents of the AI-T

The results described in Figure 3 indicated that AI-T is a large AI that migrates just below the CI holoenzyme and contains dNDUFS5 and dNDUFA11. To identify additional components of AI-T, we employed a proteomics approach. Densitometry measurements of residual CI in FAF3-kd and FAF4-kd thoraces relative to wildtype, as assessed from silver-stained gels and BN-PAGE was approximately 30% and 50% of wild-type levels, respectively (Figure S3). To examine the validity of using the label-free spectral counting approach to assess the relative abundance of subcomplexes, we quantified the relative amounts of

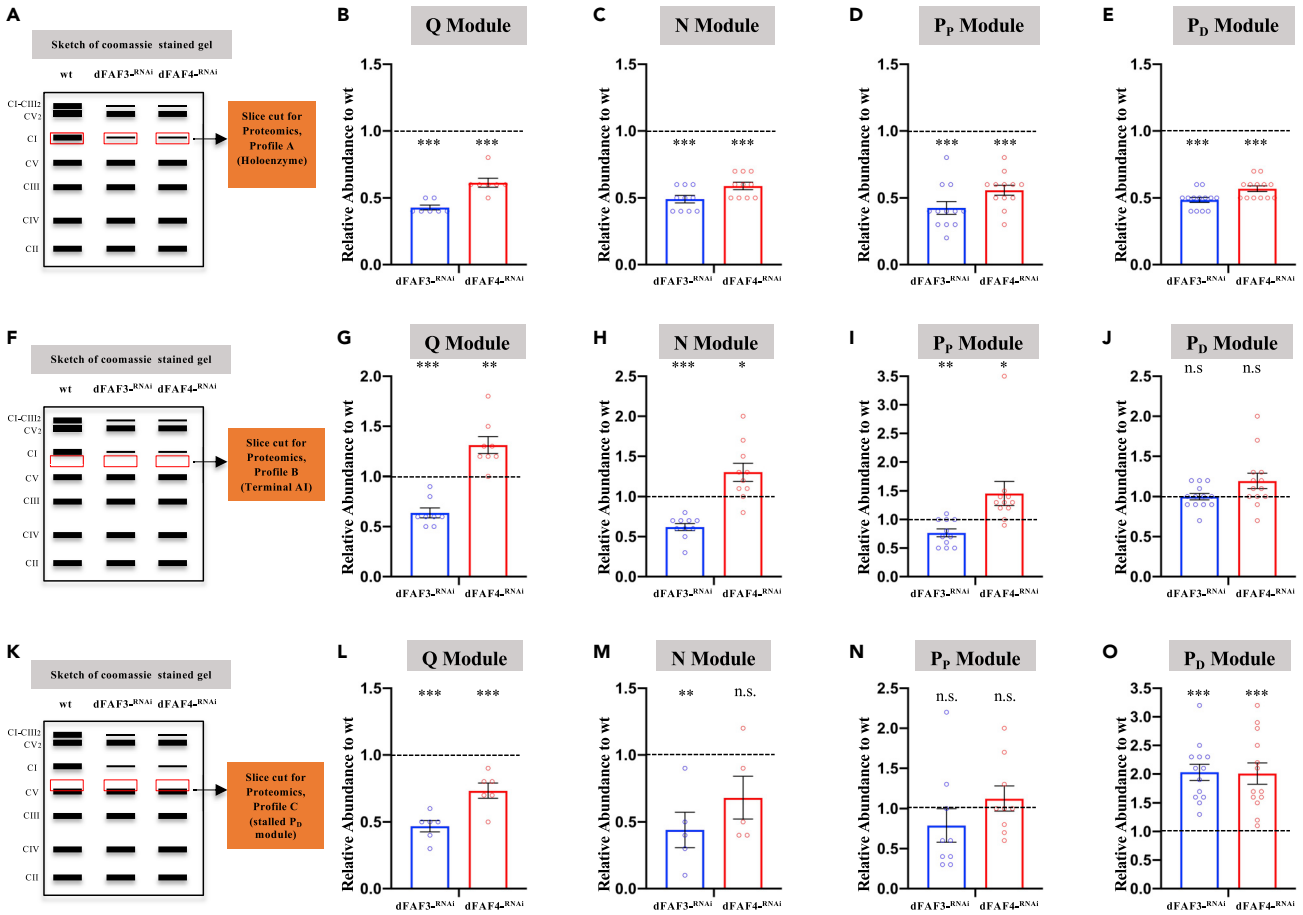

Figure 4. Proteomic analyses to identify the constituents of the terminal assembly intermediate

(A) A diagram depicting the gel slice A (corresponding to the CI holoenzyme) that was excised, and its constituent proteins analyzed by mass spectrometry.

(B–E) Label-free quantitative proteomics was used to assess the relative amount of CI subunits in the holoenzyme (gel slice A) that are part of the Q module (B), N module (C), the P_P module (D) and the P_D module (E) in mitochondrial preparations from Mhc-Gal4/UAS-dNDUFAF3^{-RNAi} and Mhc-Gal4/UAS-dNDUFAF4^{-RNAi} relative to Mhc-Gal4/w1118 (wildtype).

(F) A diagram depicting the gel slice B (corresponding to the terminal assembly intermediate) that was excised, and its constituent proteins analyzed by mass spectrometry.

(G–J) Label-free quantitative proteomics was used to assess the relative amount of CI subunits in the terminal assembly intermediate (gel slice B) that are part of the Q module (G), N module (H), the P_P module (I), and the P_D module (J) in mitochondrial preparations from Mhc-Gal4/UAS-dNDUFAF3^{-RNAi} and Mhc-Gal4/UAS-dNDUFAF4^{-RNAi} relative to Mhc-Gal4/w1118 (wild-type).

(K) A diagram depicting the gel slice C (corresponding to a stalled P_D module) that was excised, and its constituent proteins analyzed by mass spectrometry.

(L–O) Label-free quantitative proteomics was used to assess the relative amount of CI subunits in a region of the blue native gel containing a stalled P_D module and degenerating AI (gel slice C). Comparisons were made of CI subunits that are part of the Q module (L), N module (M), the P_P module (N), and the P_D module (O) in mitochondrial preparations from Mhc-Gal4/UAS-dNDUFAF3^{-RNAi} and Mhc-Gal4/UAS-dNDUFAF4^{-RNAi} relative to Mhc-Gal4/w1118 (wild-type). Note the approximately 2-fold upregulation of dNDUFC1 in (N).

In all 3 gel slices, n = 3 biological replicates with mitochondria from 20 fly thoraces per replicate; p values are based on the student's t-test for unpaired two-tailed samples. The fold change shown refers to the mean ± s.e.m (standard error of the mean); and n.s. denotes $p > 0.05$, * = $p < 0.05$, ** = $p < 0.01$ and *** = $p < 0.001$.

See also Figure S3 and Tables S1, S2, and S3.

individual subunits in the 4 CI modules of the holoenzyme from FAF3-kd and FAF4-kd samples relative to wildtype levels. Specifically, we excised a portion of the blue native gel that encompasses the CI holoenzyme (hereafter referred to as profile A) and extracted the constituent proteins (Figure 4A). Following reduction, alkylation, and trypsinization, the resulting peptides were analyzed by LC-MS/MS on an Orbitrap Fusion Lumos Tribrid mass spectrometer. Subsequently, label-free spectral counting was used to compare the relative abundance of subunits in each CI module; to obtain an average value that was used to gauge

the relative abundance of that module in the FAF3-kd and FAF4-kd samples relative to wild-type levels (Cox et al., 2014).

Our mass spectrometry technique identified all bona fide CI subunits in *Drosophila*, as well as paralogs of dNDUFS7 and dNDUFV1 (i.e. NDUFS7L and NDUFV1L, respectively, see Table S1) (Garcia et al., 2017). In addition, the residual amount of the CI holoenzyme in FAF3-kd and FAF4-kd thoraces, obtained by considering the relative abundance of all the modules of CI, was comparable to what was estimated based on the BN-PAGE and silver-stained gels (Figures 4B–4E and S3). Subsequently, we excised a portion of the blue native gel that encompasses a region just below the CI holoenzyme (hereafter referred to as profile B) (Figure 4F). This profile corresponds to the AI-T described in Figure 3G. We subjected the constituent proteins of profile B to a similar analysis as described in Figures 4A–4E. We observed that subunits in the Q, N, and P_P modules were upregulated in the AI-T found in FAF4-kd sample but downregulated in the FAF3-kd samples (Figures 4G–4I and Table S2). This is consistent with observations in Figure 3G showing that dNDUFA11 is upregulated in the FAF4-kd sample. However, while several P_D module subunits were mildly elevated in FAF4-kd samples, some subunits were reduced relative to the wild-type sample, perhaps due to ongoing degradation of the stalled AI (Figure 4J). Overall, the wave of CI biogenesis observed in profile B indicates that NDUFAF4 also regulates CI assembly at this final step.

Finally, we cut out a portion of the blue native gel just below profile B (hereafter referred to as profile C) (Figure 4K) and performed similar proteomic analyses on its constituents. The amount of the Q and N modules were decreased in both FAF3-kd and FAF4-kd samples (Figures 4L and 4M and Table S3). However, results for the P_P and P_D modules were mixed. The P_P module was not significantly altered in either the FAF3-kd or FAF4-kd samples relative to wild-type but there was a robust upregulation of the P_D module in both FAF3-kd and FAF4-kd samples (Figures 4N and 4O). While the majority of P_P module subunits were decreased, dNDUFC1 was an outlier as it was upregulated by 2-fold in both FAF3-kd and FAF4-kd samples and largely accounts for rendering the changes in the P_P module statistically insignificant (Figure 4N). The level of expression of most of the other CI subunits of the Pp module were reduced in FAF3-kd and FAF4-kd samples to a level on par with the Q and N modules (Figures 4L–4N). Because all the subunits in the P_D module are very hydrophobic, and perhaps are more refractory to proteolysis than hydrophilic subunits, the P_D module is the most stable CI AI in *Drosophila* thoraces and frequently accumulates when CI biogenesis is stalled at other modules (Figures 3H and 3I) (Murari et al., 2020; Garcia et al., 2017). Taken together, the subcomplex in profile C most likely corresponds to a stalled AI-T that is undergoing degradation, such that the amounts of the matrix domain modules (Q and N) have decreased, and most subunits in the P_P module have been degraded extensively leaving behind NDUFC1 and the relatively more stable P_D module subunits.

Multiple CIAFs associate with the residual CI and subcomplexes formed when dNDUFAF4 or dNDUFAF3 is disrupted

We used an analogous approach to what is described in Figure 4 to ascertain the degree to which CIAFs are associated with the stalled subcomplexes, or limited amount of CI formed in samples from FAF3-kd and FAF4-kd thoraces. Specifically, we carefully searched the proteomics data sets associated with the holoenzyme (profile A, Table S1), the AI-T (profile B, Table S2), and the gel slice just below the AI-T (profile C, Table S3) for CIAFs and used a label-free spectral counting approach to decipher the degree of upregulation or downregulation of each CIAF. We found that dNDUFAF3 and dNDUFAF4 were downregulated in all profiles, where they were detected in both FAF3-kd and FAF4-kd samples which is in harmony with the fact that the expression of these two CIAFs had been knocked down using RNAi (Figures 5A and 5B, also compare with Figure 1A). Interestingly, a significant amount of *Drosophila* orthologs of ACAD9 (CG9006), ECSIT (CG10610), NDUFAF1 (CG7598), TMEM126B (CG13392), TMEM186 (CG4627), FOXRED1 (CG10655), ATP5SL (CG4042), NDUFAF6 (CG15738), and TMEM70 (CG7506) were found in association with the holoenzyme, indicating that these assembly factors remain attached to the fully assembled CI holoenzyme in *Drosophila* thoraxes, at least for a time, after CI biogenesis is complete (Figures 5C–5K).

The mitochondrial complex I intermediate assembly (MCIA) complex is an inner membrane cluster of assembly factors that have a cardinal role in CI assembly. While its precise molecular function is still being unraveled, the MCIA complex is known to consist of ACAD9 (Nouws et al., 2010), NDUFAF1 (Vogel et al., 2005), ECSIT (Vogel et al., 2007), TMEM126B (Heide et al., 2012), and TMEM186 (Guerrero-Castillo et al., 2017; Formosa et al., 2020). Interestingly, we found that all 5 components of the MCIA complex

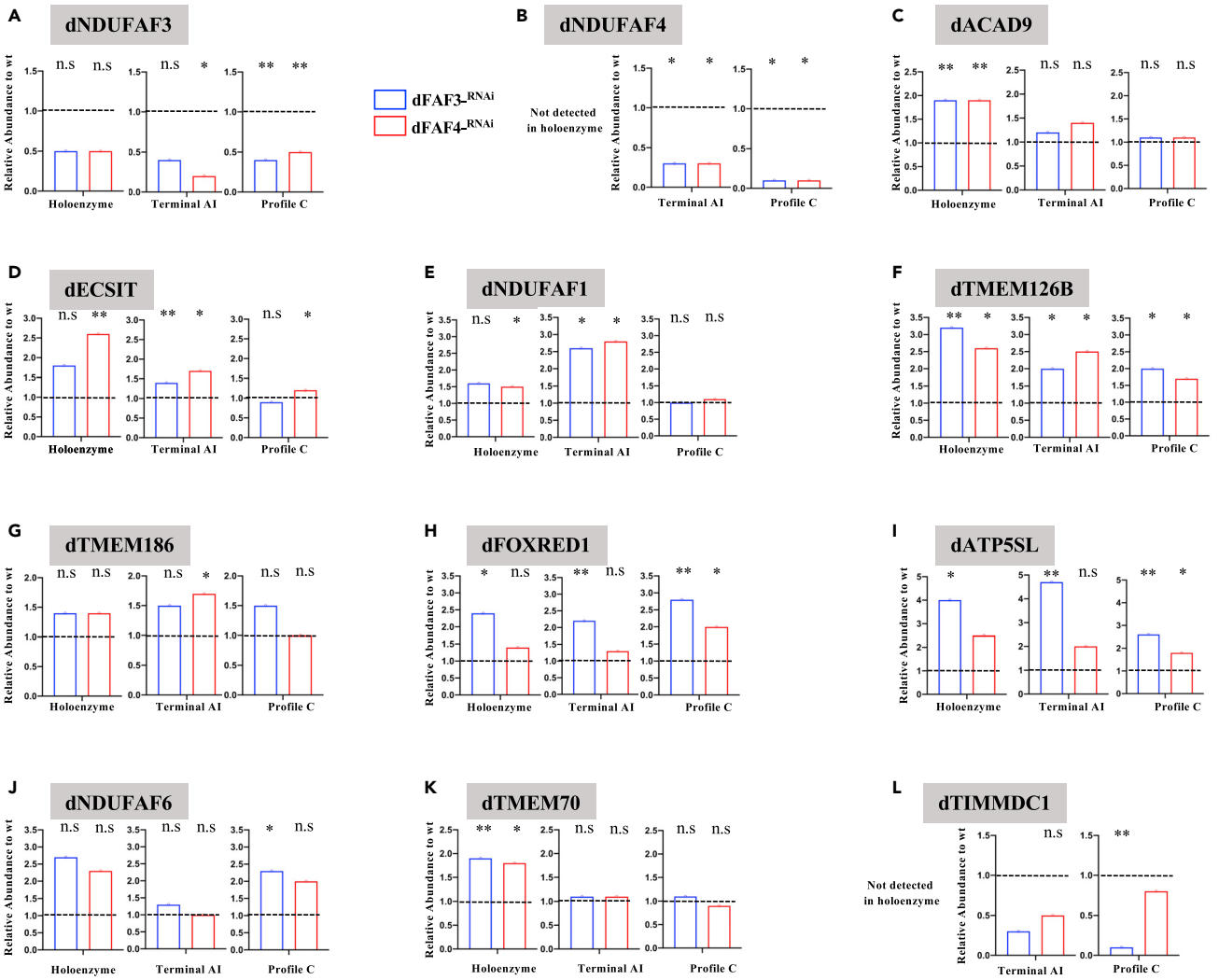

Figure 5. Multiple CI Assembly Factors accumulate while dTIMMDC1 is destabilized when dNDUFAF4 or dNDUFAF3 is disrupted

(A–L) Label-free quantitative proteomics was used to assess the relative amounts of the CIAFs shown that co-migrated with the holoenzyme (gel slice A), terminal assembly intermediate (gel slice B) and gel slice C in mitochondrial preparations from Mhc-Gal4/UAS-dNDUFAF3^{-RNAi} and Mhc-Gal4/UAS-dNDUFAF4^{-RNAi} relative to Mhc-Gal4/w1118 (wild-type).

In all instances, the fold change shown refers to the mean from 3 biological replicates, with mitochondria from 20 fly thoraces per replicate; p values are based on the student's t-test for unpaired two-tailed samples; and n.s. denotes $p > 0.05$, * = $p < 0.05$, ** = $p < 0.01$ and *** = $p < 0.001$.

See also Tables S1, S2, and S3.

were associated with subcomplexes in FAF4-kd and FAF3-kd samples (Figures 5C–5G). dFOXRED1 and dATP5SL were the only two CIAFs that were more robustly upregulated in FAF3-kd samples when compared with FAF4-kd samples across all three profiles (Figures 5H and 5I). Notably, this observation is consistent with the fact that a strong interaction was previously observed between FOXRED1 and ATP5SL immunoprecipitates, indicating that they may function together (Stroud et al., 2016). dNDUFAF6 was also found in all three profiles, suggesting that it may have additional roles in CI assembly beyond its reported role of being a cytosolic chaperone for dNDUFA10 (Figure 5J) (Zhang et al., 2013). TMEM70 was originally identified as a CV assembly factor but has now been proposed to regulate some aspects of CI assembly (Spiegel et al., 2011; Diodato et al., 2015; Guerrero-Castillo et al., 2017). Interestingly, the *Drosophila* ortholog of TMEM70 (CG7506) was also identified in all three profiles; but it only showed robust induction in association with the holoenzyme in FAF3-kd and FAF4-kd samples (Figure 5K). The general induction of assembly factors is consistent with our previous findings in Figure 1E alluding to a robust compensatory response being induced in FAF3-kd and FAF4-kd thoraces relative to wild-type. Finally, the *Drosophila*

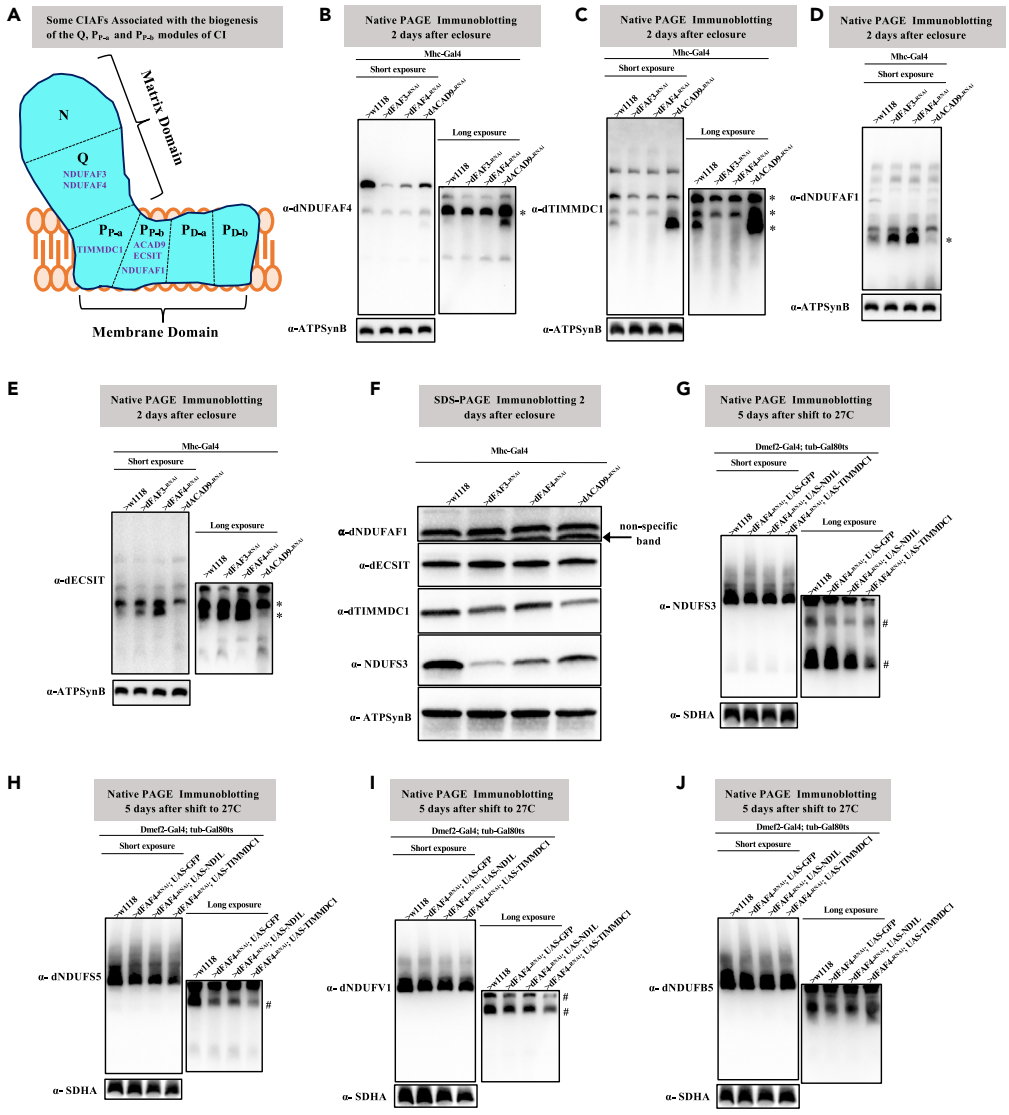

Figure 6. dNDUFAF3 and dNDUFAF4 are required for the incorporation of dTIMMDC1 into assembly intermediates

(A) An illustration of CI showing some CIAFs that regulate the biogenesis of the Q and P_P modules.

(B–E) Mitochondrial preparations from thoraces isolated from Mhc-Gal4/w1118 (wild-type), Mhc-Gal4/UAS-dNDUFAF3^{-RNAi}, Mhc-Gal4/UAS-dNDUFAF4^{-RNAi}, and Mhc-Gal4/UAS-dACAD9^{-RNAi} flies 2 days after eclosure were analyzed by BN-PAGE, followed by western blotting with antibodies raised against the CIAFs shown. The blots were imaged following a short and long exposure to detect the holoenzyme/supercomplexes and assembly intermediates respectively. The antibodies used were anti-dNDUFAF4 (B), anti-dTIMMDC1 (C), anti-dNDUFAF1 (D), and anti-dECSIT (E). Anti-ATP Synthase Beta was used as a loading control.

(F) Total cell lysates from flight/thoracic muscles isolated from Mhc-Gal4/w1118 (wildtype), Mhc-Gal4/UAS-dNDUFAF3^{-RNAi}, Mhc-Gal4/UAS-dNDUFAF4^{-RNAi}, and Mhc-Gal4/UAS-dACAD9^{-RNAi} flies 2 days after eclosure were analyzed by SDS-PAGE and anti-dNDUFAF1, anti-dECSIT, anti-dTIMMDC1, anti-NDUFS3, and immunoblotting. Anti-ATP Synthase Beta (ATP5F1B) was used as a loading control.

(G–J) Assessing whether enhanced expression of dTIMMDC1, GTPx, or NDI1 ameliorates the impaired CI biogenesis in flies expressing transgenic RNAi constructs to dNDUFAF4. Flies overexpressing GFP were included as a negative control. All flies express the tub-Gal80ts transgene, where a temperature-sensitive version of Gal80, which is active at 18°C but inactive at 27°C, is expressed ubiquitously by a tubulin promoter. Embryos expressing Dmef2-Gal4, tub-Gal80ts, and the indicated transgenes were raised at 18°C (to prevent Gal4 activity) until they eclosed as adults. Subsequently, the flies were shifted to 27°C for 5 days, to allow the RNAi constructs and overexpression constructs to be expressed.

Figure 6. *Continued*
Mitochondrial preparations were analyzed by BN-PAGE, followed by western blotting with the antibodies indicated. The antibodies used were anti-NDUFS3 which detects dNDUFS3 (G), anti-dNDUFS5 (H), anti-dNDUFV1 (I), and anti-dNDUFB5 (J). Anti-dSDHA was used as a loading control.
See also Figures S2 and S4.

ortholog of TIMMDC1 (i.e. CG9852, henceforth referred to as dTIMMDC1) was the only CIAF other than dNDUFAF3 and dNDUFAF4 that appeared to be downregulated in both AI profiles (i.e. gel slices B and C) (Figure 5L). This hinted at the possibility that dNDUFAF3 and dNDUFAF4 may regulate the stability or extent of incorporation of dTIMMDC1 in AIs. We decided to explore this hypothesis further in Figure 6.

dNDUFAF3 and dNDUFAF4 are required for the incorporation of dTIMMDC1 into AIs

The Q-module merges with the $P_{P\text{-}a}$ and $P_{P\text{-}b}$ sub-modules in the CI biosynthetic pathway (Figures S2 and 6A). TIMMDC1 is a CIAF that has been posited to regulate biogenesis of the $P_{P\text{-}a}$ sub-module as it co-migrates with $P_{P\text{-}a}$ — and Q-module subunits in native gels (Guerrero-Castillo et al., 2017; Andrews et al., 2013). TIMMDC1 also associates with the MCIA complex (Guarani et al., 2014). On the other hand, ACAD9 regulates biogenesis of some sub-assemblies in the $P_{P\text{-}b}$ sub-module. We generated antibodies to dNDUFAF4, dNDUFAF1, dECSIT, and dTIMMDC1 to explore the regulatory relationships between dNDUFAF3, dNDUFAF4, and dACAD9, and the aforementioned CIAFs. RNAi-mediated disruption of either dNDUFAF3 or dNDUFAF4 reduces the amount of dNDUFAF4 associated with subcomplexes (Figure 6B); in line with observations in Figure 1A showing that the genetic disruption of either dNDUFAF3 or dNDUFAF4 causes a reduction in both proteins. Interestingly, there was an increase in the amount of dNDUFAF4 in subcomplexes from *Mhc-Gal4/UAS-dACAD9*$^{-RNAi}$ (dACAD9-kd) samples, which is consistent with a role of dACAD9 in regulating the synthesis of the $P_{P\text{-}b}$ sub-module (Figure 6B). Accordingly, when dACAD9 is disrupted, the paucity of the $P_{P\text{-}b}$ sub-module will cause the Q/$P_{P\text{-}a}$ AI to stall and accumulate. As such, any associated CIAFs will likely accumulate, at least up to a point, before degradation by mitochondrial proteases.

Because dTIMMDC1 has also been found in association with the MCIA complex, we monitored the extent of association of dTIMMDC1, dNDUFAF1, and dECSIT with various CI AIs in samples from FAF3-kd and FAF4-kd thoraces relative to wild-type and ACAD9-kd samples. We observed that the amount of dTIMMDC1 associating with CI subcomplexes was reduced in both FAF3-kd and FAF4-kd samples, relative to wild-type samples, in line with our proteomic results from Figure 5L. This contrasts with dACAD9-kd samples where dTIMMDC1 accumulated in association with AIs (Figure 6C). Previous reports have shown that knocking out one of the components of the MCIA complex destabilizes the others (Formosa et al., 2020). In line with these observations, RNAi-mediated knockdown of dACAD9 resulted in a reduction in the amount of dNDUFAF1 and dECSIT that accumulates in AIs in ACAD9-kd samples (Figures 6D and 6E). However, both dNDUFAF1 and dECSIT accumulated in association with AIs from FAF3-kd and FAF4-kd samples (Figures 6D and 6E). We note that RNAi-mediated knockdown of dNDUFAF4 had no effect on the amount of dTIMMDC1 in total cell lysates as determined by SDS-PAGE followed by immunoblotting, while knockdown of dNDUFAF3 slightly destabilized dTIMMDC1 (Figure 6F). However, knockdown of dACAD9 notably destabilized dTIMMDC1, although an appreciable amount of dTIMMDC1 was found in association with AIs (Figures 6C and 6F). Thus, the distribution pattern of dTIMMDC1 on AIs observed in Figure 6C does not correlate with the effect of the various CIAFs on the expression level of dTIMMDC1 in total cell lysates. Consequently, we conclude that dNDUFAF3 and dNDUFAF4 regulate the stability of dTIMMDC1 in AIs.

These results are also consistent with the fact that dNDUFAF3 and dNDUFAF4 regulate biogenesis of the Q module. Thus, when dNDUFAF3 and dNDUFAF4 are disrupted, the diminished synthesis of the Q module will cause the independently formed $P_{P\text{-}b}$ module to accumulate up to a point before it is degraded by proteases. For this reason, components of the MCIA complex will initially accumulate in association with the $P_{P\text{-}b}$ module before ultimately being cleared by mitochondrial proteases. We also note that the expression levels of dECSIT and dNDUFAF1 were not altered by dNDUFAF3, dNDUFAF4, and dACAD9 in total cell lysates (Figure 6F). Thus, unlike dACAD9, genetic disruption of dNDUFAF3 and dNDUFAF4 reduces the amount of dTIMMDC1 that associates with AIs, but results in an accumulation of dNDUFAF1 and dECSIT on some AIs. These results argue strongly against dTIMMDC1 being part of the MCIA complex in *Drosophila* flight muscles.

Because disruption of dNDUFAF4 reduces the amount of dTIMMDC1 that accumulates in AIs, we investigated whether enhanced expression of dTIMMDC1 in FAF4-kd samples will rescue the CI biogenesis defects. We compared FAF4-kd samples overexpressing the following transgenes: (a) dTIMMDC1, (b) GFP (as negative controls), and (c) the alternative NADH-ubiquinone oxidoreductase (*Ndi1*). NDI1 is a single nuclear-encoded polypeptide in yeast that transfers electrons to Ubiquinone, similar to the metazoan CI. It however lacks the proton-translocating ability of the multi-subunit metazoan CI. Overexpression of the NDI1 enzyme in *Drosophila* leads to an increase in NADH–ubiquinone oxidoreductase activity, CI-dependent oxygen consumption and ATP levels (Bahadorani et al., 2010). As ROS levels are increased in FAF4-kd thoraxes (Figure 1F), we also tested whether forced expression of NDI1 could rescue some aspect(s) of the biogenesis defect in FAF4-kd samples.

We utilized the Gal4/UAS system in combination with the tub-Gal80ts system to knock down the expression of dNDUFAF4 after the flies eclosed as adults, while concurrently overexpressing the three aforementioned transgenes (Figure S4). Gal80 inhibits Gal4 activity. Therefore, the tub-Gal80ts system employs a ubiquitously expressed temperature-sensitive version of Gal80, which is active at 18°C but relatively inactive at 27°C (McGuire et al. 2004). Accordingly, embryos with the genotype Dmef2-Gal4, tub-Gal80ts/UAS-X, and UAS-dNDUFAF4RNAI were grown at 18°C until they eclosed (emerged as adults). This ensures that neither the dNDUFAF4 transgenic RNAi constructs nor the transgenes for overexpression (UAS-X) are expressed (Figure S4). After eclosure as adults, the flies were reared at 27°C for 5 days to allow the RNAi construct and overexpression transgenes to be expressed as a result of the relief of Gal4 inhibition by the temperature-sensitive Gal80 (Figure S4). Some degree of impairment of CI biogenesis was evident after 5 days at 27°C; but none of the 3 transgenes expressed could rescue the assembly defect (Figures 6G and 6H). In addition, while the effect of overexpressing NDI1 was marginal at best, forced expression of dTIMMDC1 seemed to increase the clearance of AIs as the proportion of AIs containing dNDUFS3 and dNDUFS5 were reduced relative to all other genetic manipulations (Figures 6G and 6H). As reported in Figure 2F, disruption of dNDUFAF4 had no significant effect on the dNDUFV1-containing initiating AIs. However, overexpression of dTIMMDC1 in FAF4-kd samples led to a reduction in dNDUFV1-containg AIs, as well (Figure 6I). Conversely, the amount of dNDUFB5-containing AIs, a reflection of biogenesis of the P_D module, was not appreciably different in any of the samples overexpressing the transgenes (Figure 6J). Overall, these results indicate that forced expression of TIMMDC1 in FAF4-kd samples enhances the clearance or cycling kinetics of some of the CI AIs that form in FAF4-kd samples. Thus, while the stability of dTIMMDC1 in AIs is dependent on dNDUFAF3 and dNDUFAF4, enhanced dTIMMDC1expression is not sufficient in itself to rescue the CI biogenesis defect caused by disruption of NDUFAF4. However, as we discuss later in this manuscript, this is likely part of the adaptive and compensatory stress signaling network induced as a result of disrupting dNDUFAF3 and dNDUFAF4.

Overexpression of dNDUFAF4 suppresses the diminished integration of dNDUFS3 and dNDUFS5 into CI observed when dNDUFAF3 is genetically impaired

To decipher whether the thwarted incorporation of dNDUFS3 and dNDUFS5 into CI in FAF3-kd samples can be ameliorated by overexpressing dNDUFAF4, we performed experiments analogous to what was described in Figure 6. Comparisons were made between FAF3-kd samples overexpressing the following transgenes: (a) dNDUFAF4, (b) GFP (as negative controls), (c) the yeast alternative NADH-ubiquinone oxidoreductase, NDI1, and (d) the antioxidant enzyme glutathione peroxidase (GTPx) (Missirlis et al., 2003). As ROS levels are elevated in FAF3-kd thoraxes (Figure 1F), we included NDI1 and GTPx to explore the effect of scavenging ROS levels on the phenotype observed as a result of disrupting dNDUFAF3.

After Dmef2-Gal4; tub-Gal80ts/UAS-dNDUFAF3RNAi pupae expressing the various transgenes at 18C eclosed, the flies were kept at 27°C for 5 days to allow the RNAi construct and other transgenes to be expressed. Biogenesis of AIs containing dNDUFS3 and dNDUFS5 were reduced in FAF3-kd/GFP-overexpressing samples relative to wild-type controls, indicating that the 5-day exposure to an ambient temperature of 27°C was enough to hamper ongoing biogenesis of the Q-module and $P_{P\text{-}b}$ sub-module (Figures 7A and 7B). Nevertheless, neither the overexpression of GTPx nor NDI1 was sufficient to salvage any aspect of the biogenesis defects observed in FAF3-kd samples, indicating that the increased ROS production in FAF3-kd thoraxes does not hamper CI biogenesis in these thoraxes (Figures 7A and 7B). On the other hand, forced expression of dNDUFAF4 restored the biogenesis of AIs containing dNDUFS3 and dNDUFS5 to a level at par or sometimes even exceeding wild-type levels (Figures 7A and 7B). However, overexpression of dNDUFAF4 did not alter the kinetics of dNDUFB5-containing AIs (Figure 7C).

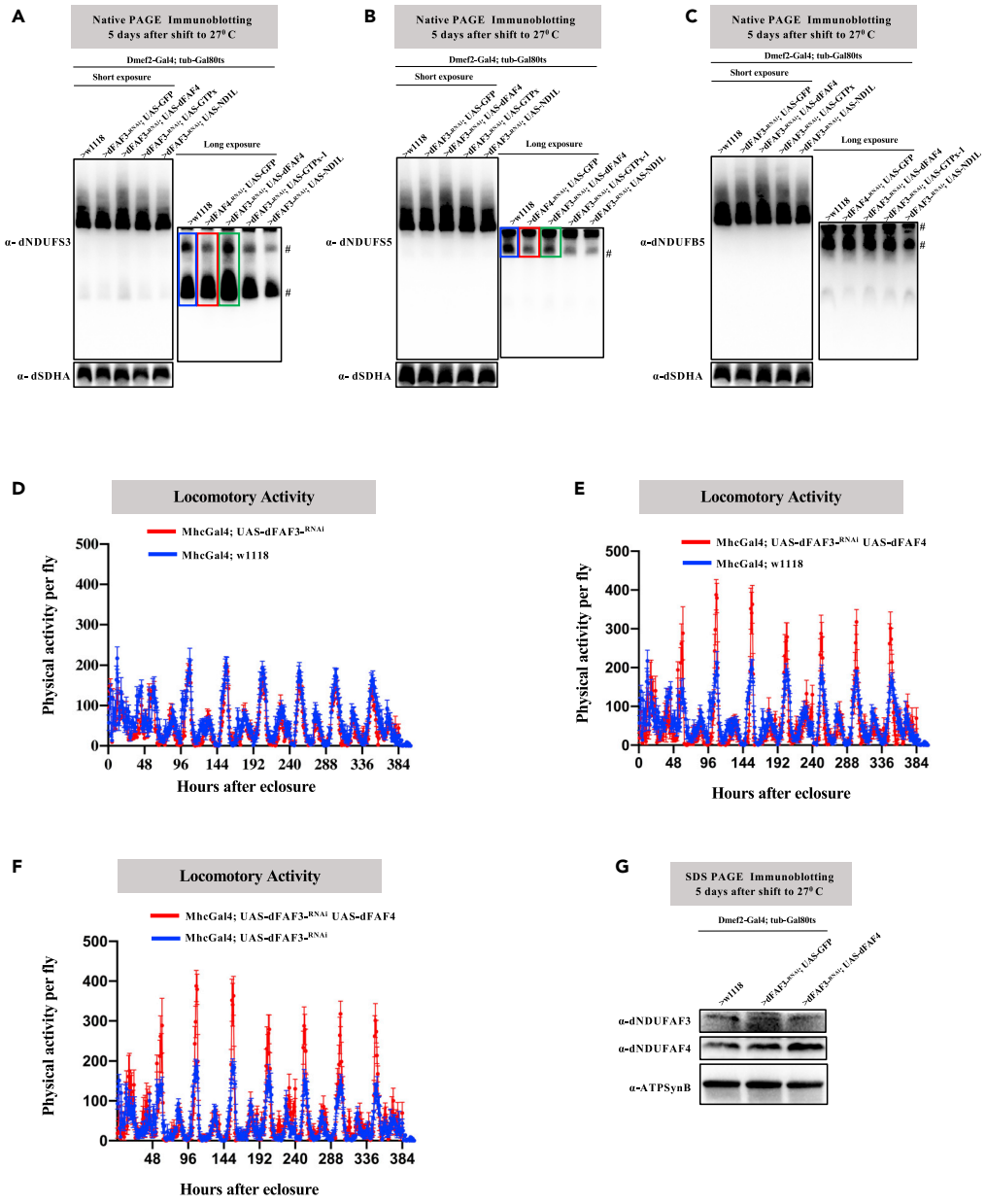

Figure 7. Overexpression of dNDUFAF4 suppresses the diminished integration of dNDUFS3 and dNDUFS5 into CI observed when dNDUFAF3 is genetically impaired

(A–C) Embryos expressing Dmef2-Gal4, tub-Gal80ts, and the indicated UAS-RNAi and overexpression transgenes were raised at 18°C until they eclosed as adults. After eclosure, the flies were shifted to 27°C to allow the transgenes to be expressed for 5 days. Subsequently, mitochondrial was prepared from all samples and analyzed by BN-PAGE, followed by immunoblotting with anti-NDUFS3 which detects dNDUFS3 (A), anti-dNDUFS5 (B), and anti-dNDUFB5 (C). Anti-dSDHA was used as a loading control. The lanes showing relevant phenotypes are demarcated in blue, red, and green.

(D–F) A comparison of the locomotory activities of Mhc-Gal4/w1118 (wild-type) and Mhc-Gal4/UAS-dNDUFAF3^{-RNAi} (D), Mhc-Gal4/w1118 (wild-type) and Mhc-Gal4/UAS-dNDUFAF3^{-RNAi}, UAS-dNDUFAF4 (E) and Mhc-Gal4/UAS-dNDUFAF3^{-RNAi} and Mhc-Gal4/UAS-dNDUFAF3^{-RNAi}, UAS-dNDUFAF4 (F) during the first 16 days after eclosure.

(G) Total cell lysates from flight/thoracic muscles isolated from samples with the genotypes shown 2 days after eclosure were analyzed by SDS-PAGE and anti-dNDUFAF3 and anti-dNDUFAF4 immunoblotting. Anti-ATP Synthase Beta (ATP5F1B) was used as a loading control.

See also Figure S4.

To evaluate the functional consequences of overexpressing dNDUFAF4 in thoraxes of FAF3-kd flies, we analyzed the spontaneous locomotory activity of FAF3-kd and FAF3-kd flies overexpressing dNDUFAF4 relative to wild-type flies over an approximately 2-week period, commencing soon after the flies eclosed. Although the spontaneous locomotory activity of the FAF3-kd flies were reduced relative to wild-type flies during the first two days post-eclosure; from the third day onward, the locomotory activity of the FAF3-kd flies were indistinguishable from those of wild-type flies, perhaps a reflection of the adaptive compensatory response induced in the FAF3-kd flies (Figure 7D). However, forced expression of dNDUFAF4 caused a potent increase in locomotory activity of the FAF3-kd flies (Figures 7E and 7F). The peak spontaneous locomotory activity of the wild-type or FAF3-kd flies did not exceed 250 units per fly within the 16 days we analyzed these results but that of the FAF3-kd flies overexpressing dNDUFAF4 consistently exceeded 300 units per fly and surpassed 400 units per fly on some occasions during the first week post-eclosure (Figures 7E and 7F). However, overexpression of dNDUFAF4 did not alter the expression of dNDUFAF3 (Figure 7G); thus the increased expression of dNDUFAF4 is sufficient to enhance the spontaneous locomotory activity of the FAF3-kd flies. Taken together, we conclude that forced expression of dNDUFAF4 in thoraxes of FAF3-kd flies enhances spontaneous locomotory activity. Consequently, these results highlight the therapeutical potential of overexpressing dNDUFAF4 in tissues where dNDUFAF3 function is impaired.

DISCUSSION

The mitochondria-enriched flight muscles of *Drosophila* are readily amenable to various genetic manipulations. Accordingly, although complete loss-of-function mutations in dNDUFAF3 and dNDUFAF4 are likely lethal in *Drosophila*; as robust RNAi-mediated disruption of either dNDUFAF3 or dNDUFAF4 in muscles fails to generate adult flies, we have been able to study the mechanism by which dNDUFAF3 and dNDUFAF4 regulate CI assembly in flight muscles. This was achieved by causing a modest disruption of these proteins in *Drosophila* flight muscles and exploring the biochemical and functional consequences.

We find that a restrained knockdown of *dNDUFAF3* and *dNDUFAF4* specifically impairs CI assembly and leads to the accumulation of some AIs. This is associated with the induction of a robust compensatory mitochondrial stress signaling network involving the upregulation of CII and CIV activity and multiple CIAFs. Given that stalled AIs are ultimately degraded by various mitochondrial proteases, their apparent stability during the early adult stage when we performed our analyses provides a window of opportunity to investigate the interdependencies of dNDUFAF3 and dNDUFAF4 on each other and the mechanism by which they regulate CI assembly.

We find that when either dNDUFAF3 or dNDUFAF4 is disrupted, the amount of dNDUFS3 and dNDUFS5 that incorporate into the Q-module and $P_{P\text{-}b}$ sub-modules, respectively, is diminished. This is associated with a destabilization of dTIMMDC1 in some AIs. The reduction in the amount of dTIMMDC1 in AIs appears to be an adaptive compensatory mechanism; as we show that enhanced expression of dTIMMDC1 decreases the steady state levels of multiple AIs. Therefore, under conditions where CI assembly is suboptimal, because dNDUFAF3 or dNDUFAF4 is genetically impaired, the system can somewhat cope with the perturbation by causing an overall retardation in the CI biosynthetic pathway by destabilizing dTIMMDC1.

Although NDUFAF3 and NDUFAF4 co-migrate in blue native gels and might be expected to act in concert during CI assembly, the AI profiles observed for these two CIAFs are not completely identical. For instance, dNDUFAF3 disruption robustly impaired the assembly of an initiating dNDUFV1-containing AI, but RNAi-mediated disruption of dNDUFAF4 did not (Figure 2F). Additionally, a higher molecular weight AI (AI-T) containing dNDUFS5 and dNDUFA11 was largely depleted in FAF3-kd samples, but remained relatively intact in FAF4-kd samples (Figures 3F and 3G). Thus, although forced expression of dNDUFAF4 rescues some aspects of the Q-module and $P_{P\text{-}b}$ sub-module defect, it is unlikely to completely rescue CI biogenesis in FAF3-kd samples. Nonetheless, a partial rescue of CI biogenesis in FAF3-kd samples by upregulation of dNDUFAF4 might have therapeutic relevance. This is because overexpression of NDUFAF4 may rescue CI assembly in cells where a point mutation in NDUFAF3 impairs its role in synthesizing the Ubiquinone module, but not the N-module and $P_{P\text{-}b}$ sub-modules where differences are observed with NDUFAF4.

We note that while dND6 and dNDUFB1 were not detected in AI-T (Table S2), it is difficult to thoroughly define the identity of AI-T as several subunits in the $P_{P\text{-}b}$ sub-module (such as dND2, dND3, and dND4L) were present at sub-stoichiometric levels. It appears the terminal AI has essentially all CI subunits incorporated to some extent but some are at sub-stoichiometric levels. Evidently, it is the last stage where the

remaining amounts of subunits that up to this point had been incorporated at sub-stoichiometric levels become fully incorporated (to stoichiometric levels) to complete the assembly process. Alternatively, some of the co-factors in the matrix domain, such as Zn^{2+}, NADPH and some Fe-S clusters may enter the complex at this point. Clearly, future studies are required to accurately establish the identity of the terminal AI.

Gene therapy is a promising approach for rectifying nuclear-encoded mitochondrial disorders. Gene therapy involving the use of adeno-associated virus vectors have been somewhat successful in remedying genetic defects in knockout mouse models of Leigh syndrome (*Ndufs4*), ethylmalonic encephalopathy, and mitochondrial neurogastrointestinal encephalomyopathy (Di Meo et al. 2012, 2017; Torres-Torronteras et al., 2011). However, given the expensive and cumbersome nature of the process, it is difficult to envisage how amending hundreds of mitochondrial genetic defects using gene therapy can become standard clinical practice in a reasonable time frame. An alternate approach is to use compounds such as bezafibrate, epicatechin, omaveloxolone, and decanoic acid which act at least in part by enhancing overall mitochondrial biogenesis to compensate for the genetic lesion (Kanabus et al. 2014; Pfeffer et al., 2012; Kanabus et al., 2016; El-Hattab et al., 2017). Our data are particularly relevant to this second approach as it may be possible to find biological agents that can upregulate the synthesis of NDUFAF4 to compensate for CI defects arising from a subset of NDUFAF3 mutations.

All things considered, our study uncovers the phenotypic spectrum associated with disrupting dNDUFAF3 and dNDUFAF4 function and sheds light on the curative potential of upregulating NDUFAF4 in tissues where CI assembly is blocked owing to a subset of genetic defects in NDUFAF3.

LIMITATIONS OF THE STUDY

We used tandem mass spectral counts in our proteomic analyses. When comparing between spectral counting and other label-free quantification approaches, spectral counting-based quantitation is more reproducible and has a larger dynamic range (Zhu, Smith, and Huang 2010). It can also tolerate higher degrees of variation in sample preparation, such as SDS-PAGE fractionation as was used in this study. However, spectral counting quantification is less sensitive. Consequently, although densitometry measurements of residual CI in FAF3-kd and FAF4-kd thoraces relative to wild-type, as assessed from silver-stained gels and BN-PAGE was approximately 30% and 50% of wild-type levels, respectively (Figure S3); the residual amount of the CI holoenzyme in FAF3-kd and FAF4-kd thoraces, obtained by considering the relative abundance of all the modules of CI using the spectral counting approach, was approximately 45% and 55% of wild-type levels, respectively (Figures 4B–4E). Thus, it appears the less sensitive spectral counting approach underestimates the extent of the decrease of CI in the FAF3-kd and FAF4-kd samples. Accordingly, what may be considered slight changes in expression levels (i.e. statistically scored as not significant) using the label-free spectral counting approach are likely to be significant changes if more sensitive assays are used. As the magnitude of expression changes obtained through the spectral counting approach are likely to be underestimated, expression changes will have to be subsequently confirmed with immunoblotting or other alternate approaches, as we confirmed with dTIMMDC1 (see Figures 5L and 6C).

STAR★METHODS

Detailed methods are provided in the online version of this paper and include the following:

- KEY RESOURCES TABLE
- RESOURCE AVAILABILITY
  - Lead contact
  - Materials availability
  - Data and code availability
- EXPERIMENTAL MODEL AND SUBJECT DETAILS
  - *Drosophila* stocks and genetics
- METHOD DETAILS
  - Locomotory activity
  - Mitochondria purification
  - Blue native polyacrylamide gel electrophoresis (BN-PAGE)
  - Silver staining
  - In-gel complex I, II, IV and V activity

- Amplex Red assay for measuring hydrogen peroxide production
- Generation of peptide polyclonal antibodies
- Immunoblotting
- In-gel digestion and mass spectrometry
- Protein identification and quantification

- QUANTIFICATION AND STATISTICAL ANALYSIS

SUPPLEMENTAL INFORMATION

Supplemental information can be found online at https://doi.org/10.1016/j.isci.2021.102869.

ACKNOWLEDGMENTS

We thank past and present members of the Owusu-Ansah lab for general discussions; Henry Colecraft, Jeanine D'Armiento, Alexander Galkin, Wes Grueber, Laura Johnston, Richard Kitsis, Andrew Marks, Martin Picard, Liza Pon, Michael Schlame, Eric Schon, and Mimi Shirasu-Hiza for fly stocks, reagents, and critical discussions. We acknowledge the Bloomington *Drosophila* Stock Center and Vienna *Drosophila* Resource Center for various fly strains and the *Drosophila* Genomics Resource Center for cDNA clones and the pUAST vector. The Drosophila Genomics Resource Center is supported by NIH grant 2P40OD010949. The mass spectrometry data were obtained from an Orbitrap mass spectrometer funded in part by NIH grants NS046593 and 1S10OD025047-01 for the support of proteomics research at Rutgers Newark campus. Work in the Owusu-Ansah lab is supported by a Provost Junior Faculty grant to support Columbia's diversity efforts, an Irma T. Hirschl Trust Scientist Award and NIH grants DK112074 (R21), AR077312 (R21), and GM124717 (R35).

AUTHOR CONTRIBUTIONS

E.O.-A conceived the project, designed all experiments, and supervised the work. A.M., S.-K.R., C.G., B.M., C.D., and E.O.-A. performed all experiments except the acquisition of the mass spectrometry data, which were performed by T.L. and H.L. A.M. and E.O.-A. analyzed and discussed results. T. L. and H.L. wrote the proteomics section of the methodology and limitations of the study. E.O.-A. wrote all other sections of the manuscript and got feedback and approval from all authors.

DECLARATION OF INTERESTS

The authors declare no competing financial interests.

Received: March 2, 2021
Revised: June 12, 2021
Accepted: July 14, 2021
Published: August 20, 2021

REFERENCES

Agip, A.A., Blaza, J.N., Bridges, H.R., Viscomi, C., Rawson, S., Muench, S.P., and Hirst, J. (2018). Cryo-EM structures of complex I from mouse heart mitochondria in two biochemically defined states. Nat. Struct. Mol. Biol. *25*, 548–556. https://doi.org/10.1038/s41594-018-0073-1. https://www.ncbi.nlm.nih.gov/pubmed/29915388.

Andrews, B., Carroll, J., Ding, S., Fearnley, I.M., and Walker, J.E. (2013). Assembly factors for the membrane arm of human complex I. Proc. Natl. Acad. Sci. U S A *110*, 18934–18939. https://doi.org/10.1073/pnas.1319247110. https://www.ncbi.nlm.nih.gov/pubmed/24191001.

Baertling, F., Sánchez-Caballero, L., Timal, S., van den Brand, M.A., Ngu, L.H., Distelmaier, F., Rodenburg, R.J., and Nijtmans, L.G. (2017a). Mutations in mitochondrial complex I assembly factor NDUFAF3 cause Leigh syndrome. Mol. Genet. Metab. *120*, 243–246. https://doi.org/10.1016/j.ymgme.2016.12.005. https://www.ncbi.nlm.nih.gov/pubmed/27986404.

Baertling, F., Sánchez-Caballero, L., van den Brand, M.A.M., Wintjes, L.T., Brink, M., van den Brandt, F.A., Wilson, C., Rodenburg, R.J.T., and Nijtmans, L.G.J. (2017b). NDUFAF4 variants are associated with Leigh syndrome and cause a specific mitochondrial complex I assembly defect. Eur. J. Hum. Genet. *25*, 1273–1277. https://doi.org/10.1038/ejhg.2017.133. https://www.ncbi.nlm.nih.gov/pubmed/28853723.

Bahadorani, S., Cho, J., Lo, T., Contreras, H., Lawal, H.O., Krantz, D.E., Bradley, T.J., and Walker, D.W. (2010). Neuronal expression of a single-subunit yeast NADH-ubiquinone oxidoreductase (Ndi1) extends Drosophila lifespan. Aging Cell *9*, 191–202. https://doi.org/10.1111/j.1474-9726.2010.00546.x. https://www.ncbi.nlm.nih.gov/pubmed/20089120.

Baradaran, R., Berrisford, J.M., Minhas, G.S., and Sazanov, L.A. (2013). Crystal structure of the entire respiratory complex I. Nature *494*, 443–448. https://doi.org/10.1038/nature11871. https://www.ncbi.nlm.nih.gov/pubmed/23417064.

Brand, A.H., and Perrimon, N. (1993). Targeted gene expression as a means of altering cell fates and generating dominant phenotypes. Development *118*, 401–415. https://www.ncbi.nlm.nih.gov/pubmed/8223268.

Cox, J., Hein, M.Y., Luber, C.A., Paron, I., Nagaraj, N., and Mann, M. (2014). Accurate proteome-wide label-free quantification by delayed normalization and maximal peptide ratio extraction, termed MaxLFQ. Mol. Cell Proteomics *13*, 2513–2526. https://doi.org/10.1074/mcp.M113.031591. https://www.ncbi.nlm.nih.gov/pubmed/24942700.

Di Meo, I., Auricchio, A., Lamperti, C., Burlina, A., Viscomi, C., and Zeviani, M. (2012). Effective AAV-mediated gene therapy in a mouse model of ethylmalonic encephalopathy. EMBO Mol. Med. *4*, 1008–1014. https://doi.org/10.1002/emmm.201201433. https://www.ncbi.nlm.nih.gov/pubmed/22903887.

Di Meo, I., Marchet, S., Lamperti, C., Zeviani, M., and Viscomi, C. (2017). AAV9-based gene therapy partially ameliorates the clinical phenotype of a mouse model of Leigh syndrome. Gene Ther. *24*, 661–667. https://doi.org/10.1038/gt.2017.53. https://www.ncbi.nlm.nih.gov/pubmed/28753212.

Diodato, D., Invernizzi, F., Lamantea, E., Fagiolari, G., Parini, R., Menni, F., Parenti, G., Bollani, L., Pasquini, E., Donati, M.A., et al. (2015). Common and Novel TMEM70 mutations in a Cohort of Italian patients with mitochondrial Encephalocardiomyopathy. JIMD Rep. *15*, 71–78. https://doi.org/10.1007/8904_2014_300. https://www.ncbi.nlm.nih.gov/pubmed/24740313.

Efremov, R.G., and Sazanov, L.A. (2011). Structure of the membrane domain of respiratory complex I. Nature *476*, 414–420. https://doi.org/10.1038/nature10330. https://www.ncbi.nlm.nih.gov/pubmed/21822288.

El-Hattab, A.W., Zarante, A.M., Almannai, M., and Scaglia, F. (2017). Therapies for mitochondrial diseases and current clinical trials. Mol. Genet. Metab. *122*, 1–9. https://doi.org/10.1016/j.ymgme.2017.09.009. https://www.ncbi.nlm.nih.gov/pubmed/28943110.

Elzakra, N., Cui, L., Liu, T., Li, H., Huang, J., and Hu, S. (2017). Mass spectrometric analysis of SOX11-Binding proteins in Head and Neck Cancer cells Demonstrates the interaction of SOX11 and HSP90α. J. Proteome Res. *16*, 3961–3968. https://doi.org/10.1021/acs.jproteome.7b00247. https://www.ncbi.nlm.nih.gov/pubmed/28915052.

Fiedorczuk, K., Letts, J.A., Degliesposti, G., Kaszuba, K., Skehel, M., and Sazanov, L.A. (2016). Atomic structure of the entire mammalian mitochondrial complex I. Nature *538*, 406–410. https://doi.org/10.1038/nature19794. https://www.ncbi.nlm.nih.gov/pubmed/27595392.

Formosa, L.E., Dibley, M.G., Stroud, D.A., and Ryan, M.T. (2018). Building a complex complex: assembly of mitochondrial respiratory chain complex I. Semin. Cell Dev. Biol. *76*, 154–162. https://doi.org/10.1016/j.semcdb.2017.08.011. https://www.ncbi.nlm.nih.gov/pubmed/28797839.

Formosa, L.E., Muellner-Wong, L., Reljic, B., Sharpe, A.J., Jackson, T.D., Beilharz, T.H., Stojanovski, D., Lazarou, M., Stroud, D.A., and Ryan, M.T. (2020). Dissecting the roles of mitochondrial complex I intermediate assembly complex factors in the biogenesis of complex I. Cell Rep. *31*, 107541. https://doi.org/10.1016/j.celrep.2020.107541. https://www.ncbi.nlm.nih.gov/pubmed/32320651.

Garcia, C.J., Khajeh, J., Coulanges, E., Chen, E.I., and Owusu-Ansah, E. (2017). Regulation of mitochondrial complex I biogenesis in Drosophila flight muscles. Cell Rep. *20*, 264–278. https://doi.org/10.1016/j.celrep.2017.06.015. https://www.ncbi.nlm.nih.gov/pubmed/28683319.

Guarani, V., Paulo, J., Zhai, B., Huttlin, E.L., Gygi, S.P., and Harper, J.W. (2014). TIMMDC1/C3orf1 functions as a membrane-embedded mitochondrial complex I assembly factor through association with the MCIA complex. Mol. Cell Biol. *34*, 847–861. https://doi.org/10.1128/MCB.01551-13. https://www.ncbi.nlm.nih.gov/pubmed/24344204.

Guerrero-Castillo, S., Baertling, F., Kownatzki, D., Wessels, H.J., Arnold, S., Brandt, U., and Nijtmans, L. (2017). The assembly pathway of mitochondrial respiratory chain complex I. Cell Metab. *25*, 128–139. https://doi.org/10.1016/j.cmet.2016.09.002. https://www.ncbi.nlm.nih.gov/pubmed/27720676.

Heide, H., Bleier, L., Steger, M., Ackermann, J., Dröse, S., Schwamb, B., Zörnig, M., Reichert, A.S., Koch, I., Wittig, I., and Brandt, U. (2012). Complexome profiling identifies TMEM126B as a component of the mitochondrial complex I assembly complex. Cell Metab. *16*, 538–549. https://doi.org/10.1016/j.cmet.2012.08.009. https://www.ncbi.nlm.nih.gov/pubmed/22982022.

Kanabus, M., Fassone, E., Hughes, S.D., Bilooei, S.F., Rutherford, T., Donnell, M.O., Heales, S.J.R., and Rahman, S. (2016). The pleiotropic effects of decanoic acid treatment on mitochondrial function in fibroblasts from patients with complex I deficient Leigh syndrome. J. Inherit. Metab. Dis. *39*, 415–426. https://doi.org/10.1007/s10545-016-9930-4. https://www.ncbi.nlm.nih.gov/pubmed/27080638.

Kanabus, M., Heales, S.J., and Rahman, S. (2014). Development of pharmacological strategies for mitochondrial disorders. Br. J. Pharmacol. *171*, 1798–1817. https://doi.org/10.1111/bph.12456. https://www.ncbi.nlm.nih.gov/pubmed/24116962.

Letts, J.A., Fiedorczuk, K., and Sazanov, L.A. (2016). The architecture of respiratory supercomplexes. Nature *537*, 644–648. https://doi.org/10.1038/nature19774. https://www.ncbi.nlm.nih.gov/pubmed/27654913.

Letts, J.A., and Sazanov, L.A. (2017). Clarifying the supercomplex: the higher-order organization of the mitochondrial electron transport chain. Nat. Struct. Mol. Biol. *24*, 800–808. https://doi.org/10.1038/nsmb.3460. https://www.ncbi.nlm.nih.gov/pubmed/28981073.

McGuire, S.E., Mao, Z., and Davis, R.L. (2004). Spatiotemporal gene expression targeting with the TARGET and gene-switch systems in Drosophila. Sci. STKE *2004*, pl6. https://doi.org/10.1126/stke.2202004pl6. https://www.ncbi.nlm.nih.gov/pubmed/14970377.

Missirlis, F., Rahlfs, S., Dimopoulos, N., Bauer, H., Becker, K., Hilliker, A., Phillips, J.P., and Jäckle, H. (2003). A putative glutathione peroxidase of Drosophila encodes a thioredoxin peroxidase that provides resistance against oxidative stress but fails to complement a lack of catalase activity. Biol. Chem. *384*, 463–472. https://doi.org/10.1515/BC.2003.052. https://www.ncbi.nlm.nih.gov/pubmed/12715897.

Murari, A., Rhooms, S.K., Goparaju, N.S., Villanueva, M., and Owusu-Ansah, E. (2020). An antibody toolbox to track complex I assembly defines AIF's mitochondrial function. J. Cell Biol *219*. https://doi.org/10.1083/jcb.202001071. https://www.ncbi.nlm.nih.gov/pubmed/32936885.

Nouws, J., Nijtmans, L., Houten, S.M., van den Brand, M., Huynen, M., Venselaar, H., Hoefs, S., Gloerich, J., Kronick, J., Hutchin, T., et al. (2010). Acyl-CoA dehydrogenase 9 is required for the biogenesis of oxidative phosphorylation complex I. Cell Metab. *12*, 283–294. https://doi.org/10.1016/j.cmet.2010.08.002. https://www.ncbi.nlm.nih.gov/pubmed/20816094.

Pagliarini, D.J., Calvo, S.E., Chang, B., Sheth, S.A., Vafai, S.B., Ong, S.E., Walford, G.A., Sugiana, C., Boneh, A., Chen, W.K., et al. (2008). A mitochondrial protein compendium elucidates complex I disease biology. Cell *134*, 112–123. https://doi.org/10.1016/j.cell.2008.06.016. https://www.ncbi.nlm.nih.gov/pubmed/18614015.

Pfeffer, G., Majamaa, K., Turnbull, D.M., Thorburn, D., and Chinnery, P.F. (2012). Treatment for mitochondrial disorders. Cochrane Database Syst. Rev. *4*, CD004426. https://doi.org/10.1002/14651858.CD004426.pub3. https://www.ncbi.nlm.nih.gov/pubmed/22513923.

Ranganayakulu, G., Schulz, R.A., and Olson, E.N. (1996). Wingless signaling induces nautilus expression in the ventral mesoderm of the Drosophila embryo. Dev. Biol. *176*, 143–148. https://doi.org/10.1006/dbio.1996.9987. https://www.ncbi.nlm.nih.gov/pubmed/8654890.

Rera, M., Bahadorani, S., Cho, J., Koehler, C.L., Ulgherait, M., Hur, J.H., Ansari, W.S., Lo, T., Jones, D.L., and Walker, D.W. (2011). Modulation of longevity and tissue homeostasis by the Drosophila PGC-1 homolog. Cell Metab. *14*, 623–634. https://doi.org/10.1016/j.cmet.2011.09.013. https://www.ncbi.nlm.nih.gov/pubmed/22055505.

Rhooms, S.K., Murari, A., Goparaju, N.S.V., Vilanueva, M., and Owusu-Ansah, E. (2019). Insights from Drosophila on mitochondrial complex I. Cell Mol Life Sci. https://doi.org/10.1007/s00018-019-03293-0. https://www.ncbi.nlm.nih.gov/pubmed/31485716.

Saada, A., Edvardson, S., Rapoport, M., Shaag, A., Amry, K., Miller, C., Lorberboum-Galski, H., and Elpeleg, O. (2008). C6ORF66 is an assembly factor of mitochondrial complex I. Am. J. Hum. Genet. *82*, 32–38. https://doi.org/10.1016/j.ajhg.2007.08.003. https://www.ncbi.nlm.nih.gov/pubmed/18179882.

Saada, A., Vogel, R.O., Hoefs, S.J., van den Brand, M.A., Wessels, H.J., Willems, P.H., Venselaar, H., Shaag, A., Barghuti, F., Reish, O., et al. (2009). Mutations in NDUFAF3 (C3ORF60), encoding an NDUFAF4 (C6ORF66)-interacting complex I assembly protein, cause fatal neonatal mitochondrial disease. Am. J. Hum. Genet. *84*, 718–727. https://doi.org/10.1016/j.ajhg.2009.04.020. https://www.ncbi.nlm.nih.gov/pubmed/19463981.

Spiegel, R., Khayat, M., Shalev, S.A., Horovitz, Y., Mandel, H., Hershkovitz, E., Barghuti, F., Shaag, A., Saada, A., Korman, S.H., et al. (2011). TMEM70 mutations are a common cause of nuclear encoded ATP synthase assembly defect: further delineation of a new syndrome. J. Med. Genet. *48*, 177–182. https://doi.org/10.1136/jmg.2010.084608. https://www.ncbi.nlm.nih.gov/pubmed/21147908.

Stroud, D.A., Surgenor, E.E., Formosa, L.E., Reljic, B., Frazier, A.E., Dibley, M.G., Osellame, L.D., Stait, T., Beilharz, T.H., Thorburn, D.R., et al. (2016). Accessory subunits are integral for assembly and function of human mitochondrial complex I. Nature *538*, 123–126. https://doi.org/10.1038/nature19754. https://www.ncbi.nlm.nih.gov/pubmed/27626371.

Sánchez-Caballero, L., Guerrero-Castillo, S., and Nijtmans, L. (2016). Unraveling the complexity of mitochondrial complex I assembly: a dynamic process. Biochim. Biophys. Acta *1857*, 980–990. https://doi.org/10.1016/j.bbabio.2016.03.031. https://www.ncbi.nlm.nih.gov/pubmed/27040506.

Torres-Torronteras, J., Gómez, A., Eixarch, H., Palenzuela, L., Pizzorno, G., Hirano, M., Andreu, A.L., Barquinero, J., and Martí, R. (2011). Hematopoietic gene therapy restores thymidine phosphorylase activity in a cell culture and a murine model of MNGIE. Gene Ther. *18*, 795–806. https://doi.org/10.1038/gt.2011.24. https://www.ncbi.nlm.nih.gov/pubmed/21451581.

Venkatesh, S., Baljinnyam, E., Tong, M., Kashihara, T., Yan, L., Liu, T., Li, H., Xie, L.H., Nakamura, M., Oka, S.I., et al. (2020). Proteomic analysis of mitochondrial biogenesis in cardiomyocytes differentiated from human induced pluripotent stem cells. Am. J. Physiol. Regul. Integr. Comp. Physiol. https://doi.org/10.1152/ajpregu.00207.2020. https://www.ncbi.nlm.nih.gov/pubmed/33112656.

Vinothkumar, K.R., Zhu, J., and Hirst, J. (2014). Architecture of mammalian respiratory complex I. Nature *515*, 80–84. https://doi.org/10.1038/nature13686. https://www.ncbi.nlm.nih.gov/pubmed/25209663.

Vogel, R.O., Janssen, R.J., Ugalde, C., Grovenstein, M., Huijbens, R.J., Visch, H.J., van den Heuvel, L.P., Willems, P.H., Zeviani, M., Smeitink, J.A., and Nijtmans, L.G. (2005). Human mitochondrial complex I assembly is mediated by NDUFAF1. FEBS J. *272*, 5317–5326. https://doi.org/10.1111/j.1742-4658.2005.04928.x. https://www.ncbi.nlm.nih.gov/pubmed/16218961.

Vogel, R.O., Janssen, R.J., van den Brand, M.A., Dieteren, C.E., Verkaart, S., Koopman, W.J., Willems, P.H., Pluk, W., van den Heuvel, L.P., Smeitink, J.A., and Nijtmans, L.G. (2007). Cytosolic signaling protein Ecsit also localizes to mitochondria where it interacts with chaperone NDUFAF1 and functions in complex I assembly. Genes Dev. *21*, 615–624. https://doi.org/10.1101/gad.408407. https://www.ncbi.nlm.nih.gov/pubmed/17344420.

Wittig, I., Beckhaus, T., Wumaier, Z., Karas, M., and Schägger, H. (2010). Mass estimation of native proteins by blue native electrophoresis: principles and practical hints. Mol. Cell Proteomics *9*, 2149–2161. https://doi.org/10.1074/mcp.M900526-MCP200. https://www.ncbi.nlm.nih.gov/pubmed/20173216.

Zhang, K., Li, Z., Jaiswal, M., Bayat, V., Xiong, B., Sandoval, H., Charng, W.L., David, G., Haueter, C., Yamamoto, S., et al. (2013). The C8ORF38 homologue Sicily is a cytosolic chaperone for a mitochondrial complex I subunit. J. Cell Biol *200*, 807–820. https://doi.org/10.1083/jcb.201208033. https://www.ncbi.nlm.nih.gov/pubmed/23509070.

Zhu, J., Vinothkumar, K.R., and Hirst, J. (2016). Structure of mammalian respiratory complex I. Nature *536*, 354–358. https://doi.org/10.1038/nature19095. https://www.ncbi.nlm.nih.gov/pubmed/27509854.

Zhu, W., Smith, J.W., and Huang, C.M. (2010). Mass spectrometry-based label-free quantitative proteomics. J. Biomed. Biotechnol. *2010*, 840518. https://doi.org/10.1155/2010/840518. https://www.ncbi.nlm.nih.gov/pubmed/19911078.

STAR★METHODS

KEY RESOURCES TABLE

REAGENT or RESOURCE	SOURCE	IDENTIFIER
Antibodies		
Rabbit polyclonal anti-dNDUFV3 (CG11752)	This paper	N/A
Rabbit polyclonal anti-dNDUFA11 (CG9350)	This paper	N/A
Rabbit polyclonal anti-dNDUFS7 (CG9172)	This paper	N/A
Rabbit polyclonal anti-dNDUFS8 (CG3944)	This paper	N/A
Rabbit polyclonal anti-dNDUFA8 (CG3683)	This paper	N/A
Rabbit polyclonal anti-dNDUFAF1 (CG7598)	This paper	N/A
Rabbit polyclonal anti-dNDUFAF3 (CG5569)	This paper	N/A
Rabbit polyclonal anti-dNDUFAF4 (CG11722)	This paper	N/A
Rabbit polyclonal anti-dTIMMDC1 (CG9852)	This paper	N/A
Rabbit polyclonal anti-dECSIT (CG10610)	This paper	N/A
Rabbit polyclonal anti-dNDUFS5 (CG11752)	Murari et al., 2020	N/A
Rabbit polyclonal anti-dNDUFV1 (CG9350)	Murari et al., 2020	N/A
Rabbit polyclonal anti-dNDUFB5 (CG9172)	Murari et al., 2020	N/A
Rabbit polyclonal anti-dNDUFB8 (CG3944)	Murari et al., 2020	N/A
Rabbit polyclonal anti-dND1 (CG7598)	Murari et al., 2020	N/A
Rabbit polyclonal anti-dND2 (CG5569)	Murari et al., 2020	N/A
Rabbit polyclonal anti-dND4L (CG11722)	Murari et al., 2020	N/A
Mouse monoclonal anti-NDUFS3	Abcam	Cat #: Ab14711 RRID: AB_301429
Mouse monoclonal anti-ATPsynβ	Life technologies	Cat #: A-21351; RRID: AB_221512
Rabbit Horseradish Peroxidase	Invitrogen	Cat #: PI31460 RRID: AB_228341
Mouse Horseradish Peroxidase	Invitrogen	Cat #: PI31430
Chemicals, Peptides, and Recombinant Proteins		
Halt protease inhibtors	Thermo Scientific	Cat #: PI78425
Digitonin	Millipore-Sigma	Cat #: D141
NativePAGE sample buffer (4X)	Invitrogen	Cat #: BN2003
NativePAGE 5% G-250 sample additive	Invitrogen	Cat #: BN2004
3–12% pre-cast Bis–Tris NativePAGE gels	Invitrogen	Cat #: BN1003BOX
NativeMark unstained protein ladder	Invitrogen	Cat #: LC0725
NativePAGE running buffer (20X)	Invitrogen	Cat #: BN2001
Nitrotetrazolium Blue Chloride (NTB)	Millipore-Sigma	Cat #: N6639
Sodium succinate	Millipore-Sigma	Cat #: S2378
Phenazine methosulfate	Millipore-Sigma	Cat #: P9625
3,3′- diaminobenzidine tetrahydrochloride (DAB)	Millipore-Sigma	Cat #: D5637
Cytochrome C from equine heart	Millipore-Sigma	Cat #: C2506
Amplex Red Reagent	Molecular Probes	Cat #: A12222
Horseradish Peroxidase	Thermo Scientific	Cat #: PI31490
microBCA kit	Thermo Scientific	Cat #: PI23235
Novex Colloidal Blue staining kit	Invitrogen	Cat #: LC6025

(*Continued on next page*)

Continued

REAGENT or RESOURCE	SOURCE	IDENTIFIER
SilverXpress silver staining kit	Invitrogen	Cat #: LC6100
Amplex Red Hydrogen Peroxide/Peroxidase Assay Kit	Molecular Probes	Cat #: A22188
EMAKYRCPQPSALK	This paper	dNDUFV3 (CG11752)
DPPKNWTTEKPKE	This paper	dNDUFA11 (CG9350)
KKVKRMKTLQMWYRK	This paper	dNDUFS7 (CG9172)
CNGDKWESEIASNLQADH	This paper	dNDUFS8 (CG3944)
TTLPEESELNVQE	This paper	dNDUFA8 (CG3683)
TFWEREKKSGYKTK	This paper	dNDUFAF1 (CG7598)
RTLRTVGRQGRN	This paper	dNDUFAF3 (CG5569)
DQKYKDTMLTQATQP	This paper	dNDUFAF4 (CG11722)
HDEKTSEHVSLDTIK	This paper	dTIMMDC1 (CG9852)
DNSSQDEHISSRQK	This paper	dECSIT (CG10610)
Experimental models: Organisms/strains		
D. melanogaster: RNAi of CG5569: y[1] v[1]; P{TRiP.HMC03468}attP40	Bloomington Drosophila Stock Center	BDSC: 51894; FlyBase: FBti0157861
D. melanogaster: RNAi of CG5569: w[1118]; P{GD10552}v21569	Vienna Drosophila Resource Center	VDRC: v21569; FlyBase: FBti0079344
D. melanogaster: RNAi of CG11722: y[1] v[1]; P{TRiP.HM05053}attP2/ TM3,Sb[1]	Bloomington Drosophila Stock Center	BDSC: 28567; FlyBase: FBti0127022
D. melanogaster: RNAi of CG11722: yw[1118]; P{GD6673}v44114	Vienna Drosophila Resource Center	VDRC: v44114; FlyBase: FBti0094849
D. melanogaster: Expresses GAL4 in muscles under control of the Mef2 promoter yw[1118]; Dmef2-Gal4	Ranganayakulu et al., 1996	Dmef2-Gal4
D. melanogaster: Expresses GAL4 in muscles under control of the Myosin heavy chain promoter. w [*]; P{w{+mC]=Mhc-RFP.F3-580}2, P{w[+mC]=Mhc-GAL4. F3-580}2/SM6b	Bloomington Drosophila Stock Center	BDSC: 38464; FlyBase: FBti0147556
D. melanogaster: Expresses temperature-sensitive GAL80 under the control of the alphaTub84B promoter. w [*]; P{w{+mC]=tubP-GAL80[ts]}10; TM2/TM6, Tb[1]	Bloomington Drosophila Stock Center	BDSC: 7108; FlyBase: FBti0027799
D. melanogaster: Expresses EGFP under UAS control w[1118]; P{w{+mC]=UAS-EGFP}34/TM3, Sb[1]	Bloomington Drosophila Stock Center	BDSC: 5430; FlyBase: FBti0013988
D. melanogaster: Expresses GTPx-1 under UAS control w[1118]; P{w{+mC]=UAS-GTPx-1}	Missirlis et al., 2003	UAS-GTPx-1
D. melanogaster: Expresses NDI1 under UAS control w[1118]; P{w{+mC]=UAS-NDI1}	Bahadorani et al., 2010	UAS-NDI1
D. melanogaster: Expresses dTIMMDC1 (CG9852) under UAS control w[1118]; P{w{+mC]=UAS-dTIMMDC1}	This paper	UAS-dTIMMDC1
D. melanogaster: Expresses dNDUFAF4 (CG11722) under UAS control w[1118]; P{w{+mC]=UAS-dNDUFAF4}	This paper	UAS-dNDUFAF4

(*Continued on next page*)

Continued

REAGENT or RESOURCE	SOURCE	IDENTIFIER
Oligonucleotides		
Short hairpin RNA sequence for CG5569: HMC03468, Table S4	Bloomington Drosophila Stock Center	N/A
Long hairpin RNAi sequence for CG5569: GD10552, Table S4	Vienna Drosophila Resource Center	N/A
Long hairpin RNAi sequence for CG11722: HM05053, Table S4	Bloomington Drosophila Stock Center	N/A
Long hairpin RNAi sequence for CG11722: GD6673, Table S4	Vienna Drosophila Resource Center	N/A
Recombinant DNA		
pUAST vector	Drosophila Genomics Resource Center	DGRC:1000;
cDNA AT14909	Drosophila Genomics Resource Center	DGRC:12046; FlyBase:FBcl0018819
cDNA LD27182	Drosophila Genomics Resource Center	DGRC:7066; FlyBase:FBcl0175312
Software and algorithms		
GraphPad Prism 8.0	GraphPad	http://www.graphpad.com/ RRID: SCR_002798

RESOURCE AVAILABILITY

Lead contact

Further information and requests for resources and reagents should be directed to and will be fulfilled by the lead contact, Dr. Edward Owusu-Ansah (eo2364@cumc.columbia.edu).

Materials availability

All antibodies and transgenic UAS constructs generated in this paper are available upon request from Dr. Edward Owusu-Ansah.

Data and code availability

- All data reported in this paper will be shared by the lead contact upon request.
- This paper does not report original code.
- Any additional information required to reanalyze the data reported in this paper is available from the lead contact upon request

EXPERIMENTAL MODEL AND SUBJECT DETAILS

Drosophila stocks and genetics

Drosophila stocks were housed in vials containing agar, molasses, yeast and cornmeal medium supplemented with propionic acid and methylparaben in humidified incubators (Forma environmental chambers) at 25°C on a 12-h:12-h dark: light cycle. For the Gal80 temperature sensitive experiments, eggs were collected and maintained at 18°C until they developed into adults and shifted to 27°C.

Transgenic RNAi stocks for disrupting dNDUFAF3/CG5569 (HMC03468) and dNDUFAF4/CG11722 (HM05053) were from the Bloomington *Drosophila* Stock Center, (BDSC). In addition, another set of transgenic RNAi stocks for disrupting dNDUFAF3/CG5569 (GD10552) and dNDUFAF4/CG11722 (GD6673) were procured from the Vienna *Drosophila* Resource Center. The sequences of the RNAi constructs are listed in Table S4

The following transgenic stocks were also used: *y w; Dmef2-Gal4* (Ranganayakulu et al. 1996), *Mhc-Gal4/SM6b* (BDSC), tubP-Gal80^{ts10} (BDSC), UAS-GFP (BDSC), UAS-GTPx (Missirlis et al., 2003), *UAS-NDI1* (Bahadorani et al., 2010). In addition, the UAS-dTIMMDC1 and UAS-dNDUFAF4 transgenic flies were generated by transforming w1118 flies with pUAST plasmids containing their respective cDNAs (LD27182 and AT14909 respectively).

METHOD DETAILS

Locomotory activity

Locomotory activity was assessed using the *Drosophila* activity monitor (TriKinetics). Specifically, 8 adult male flies were placed in the *Drosophila* activity monitor and spontaneous movements were recorded continuously for 384h on a 12-h:12-h dark: light cycle.

Mitochondria purification

Mitochondrial purification was performed essentially as described by Rera *et. al.* (Rera et al., 2011). Fly thoraxes were quickly dissected and gently crushed with a dounce homogenizer (10 strokes) in 500µl of a pre-chilled mitochondrial isolation buffer (250mM sucrose, 0.15 mM $MgCl_2$, 10mM Tris.HCl, pH 7.4) supplemented with Halt protease inhibitors (Pierce). Tissue homogenates were centrifuged twice, at 500g for 5 minutes at 4°C to remove the cuticle and other insoluble material. Subsequently, the supernatant was recovered and centrifuged at 5000g for 5 minutes at 4°C, to obtain the mitochondria-enriched pellet which was washed twice in the mitochondrial isolation buffer and stored at -80°C until further processing.

Blue native polyacrylamide gel electrophoresis (BN-PAGE)

BN-PAGE was performed using NativePAGE gels from Life Technologies, and following the manufacturer's protocol as previously described (Murari et al., 2020). The digitonin: protein ratio used was 10g digitonin: 3g of protein.

Silver staining

Silver staining of native gels was performed with the SilverXpress staining kit from Life Technologies, following the manufacturer's instructions. Briefly, gels were removed from their cassettes soon after electrophoresis, transferred into a fixative solution consisting of 50 % Methanol and 10 % Acetic acid, and rotated on a shaker for 10 minutes. Following removal of the fixative solution, a sensitizer solution (supplied with the kit) was added and kept on the shaker for an additional 20 minutes. After sensitization, the gel was washed twice with ultra-pure water for 5 minutes each. Subsequently, the gel was incubated in a staining solution (supplied with the kit) for 15 minutes on the shaker; and then washed twice with ultra-pure water for 5 minutes each. Finally, the gel was developed by adding the developer (supplied with the kit) until stained bands became apparent, at which point the reaction was terminated by the addition of the stopper solution (supplied with the kit). Images were captured with a Chemidoc imaging system (Bio-rad) within 10 minutes.

In-gel complex I, II, IV and V activity

In-gel Complex I activity was assessed by incubating the native gels in 0.1 mg/ml NADH, 2.5 mg/ml Nitrotetrazolium Blue Chloride (NTB), 5 mM Tris-HCl (pH 7.4) at room temperature for 30 mins, and overnight at 4C.

In-gel Complex II activity was assessed by incubating the native gels in 20 mM sodium succinate, 0.2 mM phenazine methosulfate, 2.5 mg/ml NTB, 5 mM Tris-HCl (pH 7.4) at room temperature for 30 mins, and overnight at 4C.

In-gel Complex IV activity was assessed by incubating the native gels in 50 mM sodium phosphate (pH 7.2), 0.05 % 3,3'- diaminobenzidine tetrahydrochloride (DAB), 50 µM of cytochrome C from equine heart at room temperature overnight.

In-gel Complex V activity was assessed by pre-incubating the gel in 35 mM Tris-base, 0.27M glycine pH 8.4 for 3 hours and then subsequently in 35 mM Tris-base, 0.27M glycine (pH 8.4), 14 mM $MgSO_4$, 0.2% w/v $Pb(NO_3)_2$ and 8 mM ATP at room temperature overnight.

Amplex Red assay for measuring hydrogen peroxide production

The amount of hydrogen peroxide produced was monitored using the Amplex Red Hydrogen Peroxide/Peroxidase Assay Kit (Catalog no. A22188, Molecular Probes). In brief, fly thoraxes were homogenized in pre-chilled mitochondrial isolation buffer supplemented with halt protease inhibitors (Pierce), and centrifuged twice at 500g for 5 minutes at 4°C to remove insoluble material. Subsequently, a serial dilution of the supernatant was added to a reaction buffer containing 100uM Amplex Red Reagent and 0.2U/ml Horseradish Peroxidase solution. Fluorescence was measured at an excitation wavelength of 540nm and

detected at 590nm every 30 sec for 30 min at 25°C using a SpectraMax paradigm multi-mode microplate reader (Molecular Devices). The background fluorescence determined for a no H_2O_2 reaction was deducted from each value. Amplex Red activity was normalized to protein concentrations as determined with a microBCA kit (Thermo Fisher Scientific, Waltham, MA).

Generation of peptide polyclonal antibodies

Rabbit polyclonal antibodies recognizing various segments of specific target proteins in *Drosophila* were generated using the synthetic peptides listed below:

Peptide antigen: EMAKYRCPQPSALK	Target Protein: dNDUFV3 (CG11752)
Peptide antigen: DPPKNWTTEKPKE	Target Protein: dNDUFA11 (CG9350)
Peptide antigen: KKVKRMKTLQMWYRK	Target Protein: dNDUFS7 (CG9172)
Peptide antigen: CNGDKWESEIASNLQADH	Target Protein: dNDUFS8 (CG3944)
Peptide antigen: TTLPEESELNVQE	Target Protein: dNDUFA8 (CG3683)
Peptide antigen: TFWEREKKSGYKTK	Target Protein: dNDUFAF1 (CG7598)
Peptide antigen: RTLRTVGRQGRN	Target Protein: dNDUFAF3 (CG5569)
Peptide antigen: DQKYKDTMLTQATQP	Target Protein: dNDUFAF4 (CG11722)
Peptide antigen: HDEKTSEHVSLDTIK	Target Protein: dTIMMDC1 (CG9852)
Peptide antigen: DNSSQDEHISSRQK	Target Protein: dECSIT (CG10610)

Immunoblotting

Immunoblotting was performed as previously described (Murari et al., 2020). The primary antibodies used were anti-NDUFS3 (abcam, ab14711), anti-dNDUFS5 *(Murari et al. 2020)*, anti-dNDUFV1 (Murari et al., 2020), anti-dNDUFB5 (Murari et al., 2020), anti-dNDUFB8 (Murari et al., 2020), anti-dND1 (Murari et al., 2020), anti-dND2 (Murari et al., 2020), anti-dND4L (Murari et al., 2020), anti ATPsynß (Life technologies, A21351) and the new rabbit polyclonal antibodies generated by Biomatik. Secondary antibodies used were goat anti-rabbit Horseradish Peroxidase (PI31460 from Pierce) and goat anti-mouse Horseradish Peroxidase (PI31430 from Pierce).

A commercially available marker [i.e. the NativeMark Protein standard (Life Technologies)], which is a soluble protein marker, was initially used to estimate the molecular weight of the protein complexes. We show one example in Figure S1. However, there are major discrepancies between the migration behavior of membrane and soluble protein markers (Wittig et al., 2010). In Figure S1 shown, CV migrates with a size of ~720 kDa although CV should migrate at ~550 kDa. Indeed, none of the other OXPHOS complexes were adjudged to migrate at their appropriate sizes using this protein marker. Accordingly, estimating the sizes of membrane proteins such as OXPHOS complexes or assembly intermediates on blue native gels using standard soluble protein markers produces spurious results. Due to these discrepancies, where possible, the identity of OXPHOS complexes and assembly intermediates in immunoblots were assessed based on their position in the gel and known constituent protein subunits.

In-gel digestion and mass spectrometry

OXPHOS complexes from mitochondrial preparations from three genotypes [Mhc-Gal4/w1118 (wildtype), Mhc-Gal4/UAS-dNDUFAF3^{-RNAi}, and Mhc-Gal4/UAS-dNDUFAF4^{-RNAi} flies] were separated on blue native gels. Each sample was run in triplicate. Following resolution of the OXPHOS complexes, the gel was incubated in a fixative consisting of 50% methanol, 10% acetic acid and 100mM ammonium acetate for 30 minutes. Subsequently, the gel was washed twice with ultrapure water, and three gel slices corresponding to the holoenzyme, AI_T and a region just below the AI_T were excised for each genotype. The excised gel slices were further diced into smaller pieces, placed in eppendorf tubes, and de-stained in a gel de-staining buffer (8% Acetic acid). In-gel trypsin digestion was performed essentially as described previously (Elzakra et al., 2017). In brief, 100µl of 25mM DTT and 100µl of 50mM iodoacetamide were used for protein reduction and alkylation respectively, followed by digestion with 0.5 µg of trypsin at 37 °C for 16 h. The tryptic peptides were extracted and desalted using a C_{18} cartridge, followed by LC-MS/MS analysis on an Orbitrap Fusion Lumos Tribrid mass spectrometer (MS) (Thermo Scientific). The peptides were separated on a C_{18} nano column (75 µm × 50 cm, two µm, 100 Å) with a 2-h linear-gradient consisting of solvent A (2% acetonitrile in 0.1% formic acid (FA)) and solvent B (85% acetonitrile in 0.1% FA). The eluted peptides

were directly introduced to the MS *via* a nanospray Flex ion source. The MS spectra were acquired in the positive mode with a spray voltage of 2 kV. The temperature of the ion transfer tube was 275 °C. MS scan range was between m/z 375 and 1,500 with a 120,000 (FWHM) resolution in the Orbitrap MS. The peptides with charge states between 2 and 7 were selected for MS/MS analysis. Higher-energy Collisional Dissociation (HCD) was used for peptide fragmentation with the collision energy of 30%.

Protein identification and quantification

The MS/MS spectra were searched against the Uniprot *Drosophila* database (21,107 entries, downloaded on 11/12/2020) using the Sequest search engine through the Proteome Discoverer (version 2.4) platform. The mass tolerance was 10 ppm for MS and 0.6 Da for MS/MS. Methionine oxidation and N-terminus acetylation were set as variable modifications, and cysteine carbamidomethylation was set as a fixed modification. The false discovery rate accepted for the identification of both proteins and peptides was less than 1%. Relative protein quantitation was calculated based on the spectral counting (SC) method (Venkatesh et al., 2020; Cox et al., 2014). To circumvent the problem with large SC ratios from small spectra counts in the SC ratio denominators, we arbitrarily added 2 SC for each protein before calculating the protein quantification ratios.

QUANTIFICATION AND STATISTICAL ANALYSIS

Except where noted , p values are based on the student's t-test for unpaired two-tailed samples. The fold change shown refers to the mean $\pm$ s.e.m (standard error of the mean); and * = $p<0.05$, ** = $p<0.01$ and *** = $p<0.001$.